AD NUMBER

AD802526

LIMITATION CHANGES

TO:

Approved for public release; distribution is unlimited.

FROM:

Distribution authorized to U.S. Gov't. agencies and their contractors; Critical Technology; NOV 1966. Other requests shall be referred to Air Force Arnold Engineering Development Center, AETS, Arnold AFB, TN. This document contains export-controlled technical data.

AUTHORITY

usaedc ltr, 23 jan 1975

Unclassified

AEDC-TR-66-182

RADAR STUDY OF SPHERE WAKES

R. E. Hendrix and A. B. Bailey

ARO, Inc.

November 1966

VON KÁRMÁN GAS DYNAMICS FACILITY
ARNOLD ENGINEERING DEVELOPMENT CENTER
AIR FORCE SYSTEMS COMMAND
ARNOLD AIR FORCE STATION, TENNESSEE

Unclassified

NOTICES

When U. S. Government drawings specifications, or other data are used for any purpose other than a definitely related Government procurement operation, the Government thereby incurs no responsibility nor any obligation whatsoever, and the fact that the Government may have formulated, furnished, or in any way supplied the said drawings, specifications, or other data, is not to be regarded by implication or otherwise, or in any manner licensing the holder or any other person or corporation, or conveying any rights or permission to manufacture, use, or sell any patented invention that may in any way be related thereto.

Qualified users may obtain copies of this report from the Defense Documentation Center.

References to named commercial products in this report are not to be considered in any sense as an endorsement of the product by the United States Air Force or the Government.

RADAR STUDY OF SPHERE WAKES

R. E. Hendrix and A. B. Bailey
ARO, Inc.

AF - AEDC
Arnold AFS Tenn

FOREWORD

The research reported herein was sponsored by the Arnold Engineering Development Center (AEDC), Air Force Systems Command (AFSC), under Program Element 65402234. The results of the research presented were obtained by ARO, Inc. (a subsidiary of Sverdrup & Parcel and Associates, Inc.), contract operator of AEDC, Arnold Air Force Station, Tennessee, under Contract AF40(600)-1200. The experimental data were obtained between January and December 1965 under ARO Project Numbers VK3080 and VT2629, and the manuscript was submitted for publication on August 29, 1966.

The authors are indebted to their colleagues for their assistance during this investigation: D. A. Mayfield and R. C. Hensley for their work on the design and operation of the microwave equipment, O. H. Bock for the design and successful operation of the schlieren system, and A. J. Cable and J. Blanks for their work on the development of model launch techniques. Finally the authors are particularly indebted to P. L. Clemens and J. Leith Potter for suggestions and encouragement in the course of this work.

This technical report has been reviewed and is approved.

Donald E. Beitsch
Major, USAF
AF Representative, VKF
Directorate of Test

Leonard T. Glaser
Colonel, USAF
Director of Test

ABSTRACT

A series of firings was executed in the 100-ft Range K of the VKF for the purpose of determining the causes of radar reflections from the wakes of hypervelocity spheres. A 35-kmc, focused, oblique radar was employed as the primary instrumentation. In addition, receiving and parasite antennas were used to measure transmission and specular reflection. The results of these experiments indicate that, when using the 35-kmc microwave equipment described here, a detectable radar reflection in most cases was obtained from the wake of a hypervelocity sphere (10,000 to 27,000 ft/sec in these experiments) only if the sphere ablated. Measurements of turbulent wake velocity were shown to agree with the predicted values. The region of transition from laminar to turbulent flow was also defined.

CONTENTS

ILLUSTRATIONS

TABLES

NOMENCLATURE

C	Specific heat, Btu/lb/°K
D	Diameter of lens aperture
d	Diameter of sphere
f	Focal length
K	Thermal conductivity, Btu/sec/ft^2/°K/ft
M	Mach number
p	Pressure
r	Nose radius, ft
S	Flight distance, ft
T	Temperature, °K

ΔT	Temperature - 300, °K
V_w	Wake Velocity
$(V/\nu)_\infty$	Unit Reynolds number
w	Viscous wake width
w_i	Inviscid wake width
x	Axial distance
y	Radial distance
λ	Free space wavelength
ρ	Density, lb/ft^3
ν	Kinematic viscosity

SUBSCRIPTS

M	Melting
tr	At wake transition
∞	Free-stream conditions

SECTION I
INTRODUCTION

The launchings of spheres in the 100-ft hypervelocity Range K (Armament Test Cell, Hyperballistic (K)) in the von Kármán Gas Dynamics Facility (VKF) have been periodically monitored by a 35-kmc, oblique, focused radar. The focused antennas employed in the radar were evaluated during the initial launchings, and then a series of firings was begun for the purpose of systematically varying model materials, speeds, and range pressures while observing radar returns from the wakes of hypervelocity spheres. This aspect of the subject is not widely reported in the literature, and the necessity for accurate interpretation of future radar data dictated this program of experimental investigation. It was hoped that a better understanding of reflection phenomena would be gained and would also aid in the analysis of data resulting from the application of other wake diagnostic techniques, e.g., resonant cavities and transverse microwave probes.

SECTION II
APPARATUS

A description of Range K can be found in Ref. 1. Range K consists of the following components:

2.1 LAUNCHER

The launcher is a two-stage, light gas gun consisting of a combustion chamber, pump tube, high pressure section, and launch tube. Various high pressure sections are employed, and launch tubes ranging in diameter from 0.375 to 1.0 in. have been used with this launcher. To protect the model in the launch tube, it is mounted in a Lexan® sabot. The two main types of sabots used are discussed in Ref. 1.

2.2 BLAST AND RANGE TANKS

Both of these tanks are 6-ft-diam cylinders joined by a short spool piece containing a high vacuum valve which permits pressure isolation of the two tanks.

The blast tank is 12 ft long and has a series of ports along the sides and upper surface to permit X-ray photographs to be taken of the model

and sabot after they have left the launch tube. The range tank is 103 ft long and is equipped with six dual-axis shadowgraphs installed at approximately 15-ft intervals. There is also a high sensitivity, single-pass schlieren system which is used to study body flow fields over a wide range of model flight conditions. This system can be operated with a vertical or horizontal, servo-controlled knife edge, with a vertical or horizontal Wollaston birefringent prism, or as a focused shadowgraph. When a single-flash spark source is used, the flow field is photographed with a Speed Graphic® camera. A Strobokin® multi-spark light source is used in conjunction with a high-speed drum camera to study the far wakes of high speed bodies. Using this latter arrangement, as many as twenty frames can be photographed during a single shot.

2.3 MICROWAVE INSTRUMENTATION

The backscattered signals from the wakes of high speed spheres were monitored with a 35-kmc oblique Doppler radar. A schematic of the radar head is shown in Fig. 1. The antenna is located in the range tank and is mounted at an angle of 45 deg to the longitudinal axis of the range. The sensitivity of the radar shown in Fig. 1 could be increased by adding stages of microwave amplification and by employing i-f stages; however, for the purpose of the test work described here, the circuitry shown in Fig. 1 was considered to be adequate. A schematic of the complete radar installation, including the transmitter and the receiving and parasite antennas, is shown in Fig. 2. The signals entering the receiving and parasite antennas were detected and d-c coupled to recording oscilloscopes. The focusing antennas employed in the radars consisted of conical horns, phase-corrected with dielectric lenses. The transmitting antenna, shown in Figs. 1 and 2, was equipped with a lens having a focal length of 24 in. and f/D ratio of 4. Laboratory measurements of the antenna patterns of this particular horn-lens combination made using 0.175-in.-diam spherical targets, indicated an E-plane, 3-db beam width of 6λ (2.02 in. at 35 kmc), an H-plane 3-db beam width of 8λ (2.7 in. at 35 kmc), and an H-plane, 10-db beam width of 11λ (3.7 in. at 35 kmc). The antenna is oriented such that the E-plane is parallel to the model flight axis, as shown in Fig. 2. Therefore, when this antenna is used in the oblique radar system with a viewing angle of 45 deg, the distance traveled by a sphere during passage through the beam is $2.02\sqrt{2} = 2.85$ in., between the 3-db points.

However, the antenna focusing property of most interest in the aerophysical measurements discussed in this report is the total effective beam width, i.e., the total distance along the flight axis during which discernible radar signals are obtained from the model. This effective

value of beam width is therefore a function of the sensitivity of the radar and its readout system, in addition to the focusing properties and viewing angle of the antenna and the reflectance properties of the model* and its flow field. The sensitivity is limited by the inherent radar and readout system noise levels, which remain fairly constant for a given system. The minimum detectable reflected signal (a measure of the radar sensitivity) from a sphere for a radar operating at a given noise level is a function of the microwave illumination intensity† on the sphere and of the diameter and material and surface properties of the sphere. Summarizing, the total effective beam width, as defined above, is determined primarily by the focusing properties and viewing angle of the antenna, the intensity of microwave illumination on the sphere, and by the reflectance properties of the sphere.

A typical dynamic value of the total effective beam width is illustrated in Fig. 3a by a radar record which indicates that discernible reflections were obtained from a nonablating aluminum sphere for a distance of 4.65 in. along the flight axis. It is also shown in Fig. 3a that the sphere traveled 2.87 in. along the flight axis between the 3-db points in the microwave beam, which corresponds to a 3-db beam width of 2.03 in. (i. e., $2.87/\sqrt{2}$) in the E-plane. The value of 3-db beam width, 2.03 in., agrees well with the value of 2.02 in. measured in the laboratory, using a target having a projected area of 0.16 of that of the sphere represented in Fig. 3a. This is indicative of the well-focused character of the microwave beam. The experimental value of 3-db beam width shown in Fig. 3a was obtained from the 6-db points on the Doppler record because the amplitude of the Doppler signal is proportional to the square of the true beam field intensity, assuming a square-law detector response (Ref. 2). The total effective beam width shown in Fig. 3a (namely, 4.65 in.) is approximately equal to the E-plane, 10-db beam width projected on the flight axis.

---

*The reflectance properties of concern here are model size, surface material, and surface roughness.

†While the sphere is in the microwave beam, the intensity of illumination on the sphere is not only a function of the model position in the E-plane of the microwave beam, i. e., along the range centerline, but also its position in the H-plane of the beam and its position along the optical axis of the beam.

SECTION III
ABLATION PREDICTIONS BASED ON TEMPERATURE AT STAGNATION POINT

The temperature at the body stagnation point is of interest since it is an indication of whether or not the model under test might ablate. It has been shown (Ref. 3) that the temperature rise at the stagnation point caused by the aerodynamic heating is given by

$$\Delta T = 10(V_\infty/10^4)^{2.65}[(\rho_\infty/760)(S/r)(1/\rho CK)]^{1/2} \quad (1)$$

(The system of units is defined in the nomenclature.) This equation is based on the solution of the unsteady heat conduction equation for a sphere under the following conditions: (1) initial ambient temperature of 300°K throughout the model, (2) constant heat-transfer rate to the sphere, (3) short flight times, and (4) no model rotation. The properties of some of the materials likely to be used in aeroballistic range work are listed in Table I. Figure 4 and Table I permit calculation of the flight distance required for a sphere to reach melting temperature at the stagnation point.

In the present investigation the microwave equipment was located approximately 40 ft from the muzzle of the gun. Using this distance and the data given in Fig. 4 and Table I, the predicted results pertaining to the present study are shown in Fig. 5. Equation (1) shows that for a particular material, length of flight path, and velocity, the pressure at which ablation is likely to occur is directly proportional to the model diameter. This relationship is illustrated by the curves for aluminum spheres shown in Fig. 5. It is encouraging to note that a calculation mentioned by Kornegay (Ref. 4) for a 0.187-in.-diam aluminum sphere, traveling at 18,000 ft/sec for a distance of 45 ft, is in good agreement with the present calculations (Fig. 5).

SECTION IV
DISCUSSION OF RESULTS

4.1 COMPARISON OF PREDICTED ABLATION ONSET WITH RADAR SIGNALS

The above calculations should be considered as depicting conditions under which the possibility of ablation cannot be overlooked. For example, a series of 0.125-in.-diam steel spheres has been launched at speeds of approximately 17,300 ft/sec into an ambient pressure of 200 mm Hg. Reference to Fig. 5 indicates that model ablation under

these conditions would be likely. A simple ballistic spectrograph indicated the presence of iron in the flow field around these models. Figure 3c indicates a radar return from the wake of such a model. A 0.125-in. -diam tungsten carbide sphere fired under similar conditions produced no radiation which could be detected by the ballistic spectrograph and no wake reflections which the radar could detect (Fig. 3d). Figure 5 indicates that, at a velocity of 17,300 ft/sec, a pressure on the order of 300 mm Hg would be required to produce ablation of the tungsten carbide sphere.

To determine whether there is a relationship between a radar wake return and the likelihood of model ablation, the radar returns for a variety of materials and flight conditions (listed in Table II) are compared in Fig. 6. These comparisons suggest that a radar wake return most often was obtained whenever the model and shot conditions were such that the melting temperature boundary was approached.

Figure 7 represents a 0.125-in. -diam copper sphere launched at 26,200 fps and a range pressure of 19.6 mm Hg with no sign of transition in the visible wake. Unfortunately, no similar schlieren record is available for a 0.25-in. -diam sphere, but, based on Ref. 5, it can be shown that the 0.25-in. sphere at the same conditions should have a laminar wake for approximately 23 body diameters. On the same basis, the 0.125-in. sphere should have a laminar wake for roughly 46 body diameters. Figure 6a indicates that a 0.25-in. -diam aluminum sphere launched at this speed and pressure should be considered as likely to ablate. The oblique radar and receiving antenna records are shown in Figs. 8a and b for a shot of this type (Shot K-1408). Also shown in Fig. 8c is the parasite antenna record for another similar shot (Shot K-1415, Table II).

The oblique radar record (Fig. 8a) indicates that there is a low frequency return from the wake indicating a reflecting source velocity about 40 times slower than that indicated in Fig. 3c for a turbulent wake. The receiving antenna (Fig. 8b) indicates that the transmitted signal is completely cut off for approximately 400 μsec. If, as would be inferred from the schlieren observations (Ref. 5) the wake is laminar for roughly 23 diameters or 18 μsec, then a specular reflection of the microwave energy would be expected for that time. Figure 8c indicates that the parasite antenna located to monitor specular reflection detected a reflected signal for approximately 400μsec. Thus, under these conditions (0.25-in. -diam aluminum sphere at 26,000 ft/sec at a pressure of 20 mm Hg), the wake is opaque to microwave energy and either wholly laminar for a greater time or distance than one would expect, or the possibly turbulent inner wake is shielded from microwave interaction by ablation products. This points to an influence of ablation on microwave signals which cannot be detected by a simple backscatter system.

Figure 6 d indicates that a 0.125-in. -diam copper sphere at 26,000 ft/sec and a pressure of 20 mm Hg would not be likely to ablate, and Fig. 6a indicates that a 0.125-in. -diam aluminum sphere at the same conditions would ablate. In Fig. 9 the receiving and parasite antenna records from two such shots are compared. For the copper model (Fig. 9a) both antennas recorded the passage of the model only; whereas for the aluminum model (Fig. 9b), a strong signal was received from the wake on both antennas. This tends to confirm the conclusion drawn earlier that at this microwave frequency and at these shot conditions, the products of ablation appear to have provided the source of reflection for the microwave energy from the wakes.

Figure 10 presents the experimentally measured variation of electron density with ambient pressure and velocity in the wakes of nonablating spheres (Ref. 6). For the model and flight conditions listed in Table II, Fig. 10 indicates that the wake electron density was always less than 10^{12} cm^{-3} when $x/d \geq 40$. Heald and Wharton (Ref. 7) show that when the wake electron density is equal to or greater than the cutoff electron density at the particular microwave frequency (overdense condition), the plasma reflection coefficient is close to unity. When the wake electron density is an order of magnitude less than the cutoff value (underdense), then the reflection coefficient is on the order of 0.01. Thus, in the overdense case a strong backscattered signal would be expected. The conditions for all shots listed in Table II are such that the electron density in the wake of a nonablating body is always an order of magnitude less than the cutoff value for a 35-kmc system ($1.24 \times 10^{13}/cm^3$), as inferred from Ref. 6 and shown in Fig. 10. Therefore, it would not be expected that the present radar system could detect any strong backscattered signals from the wakes of the nonablating spheres.

Listed in Table II are some results obtained with nylon spheres. A melting boundary curve has not been derived for this material because there is uncertainty in the definition of melting temperature for all such thermoplastics. However, the results of some low speed shots with this material are of interest. In Fig. 3b it can be seen that there is a backscattered signal from the wake of a nylon sphere at a velocity of 10,500 ft/sec and a pressure of 99 mm Hg. Ablation at these flight conditions was initiated by firing the sphere into a blast tank pressure of 600 mm Hg to induce early ablation. From there the sphere passed through a diaphragm into the lower pressure in the range. Aluminum models (Table II; shots 1270, 1272, 1273, and 1274) launched at similar pressures and velocities gave no evidence of any return from the wake. Therefore, under these conditions, the radar return from the wake indicated in Fig. 3b again can be associated with the presence of the products of ablation.

4.2 EFFECTIVE RADAR WAKE DIAMETER

The diameter of the focused microwave beam at the 10-db points in the H-plane was determined experimentally in the laboratory to be 3.7 in. For complete cutoff of transmission, as shown in Fig. 8b, the wake diameter has to be equal to at least 3.7 in. The wake behind a 0.125-in.-diam aluminum sphere (Fig. 9b) does not indicate complete cutoff. However, this smaller wake still appeared opaque to the microwave energy, as evidenced by the attenuation in the receiver output which indicated approximately 50 percent of complete cutoff. The microwave signal is attenuated to this 50-percent level for approximately 500 body diameters, which compares favorably with the cutoff length for the 0.25-in.-diam models (Fig. 8b).

It is of interest to consider the diameters of some of the relevant fluid dynamic flow field regions to determine the zones of the flow field where the products of ablation are confined. The viscous and inviscid wakes and the bow shock wave shape are defined in Fig. 11, and some values for their dimensions, derived from Ref. 5, are shown in Fig. 12 for a particular set of test conditions. It will be noted that the diameters of the viscous and inviscid wakes are almost equal for these conditions when $50 \leq x/d \leq 1000$. However, the viscous wake diameter has been derived from data where turbulence is known to occur close to the body. Figure 12 suggests that for Shot K-1408 the diameter of the reflecting source in the wake of the sphere was greater than the viscous and inviscid wake diameters and, in fact, appears to have approached the bow shock wave boundary. This indicates, at least for this flight condition, that the products of ablation were not confined to the inviscid or viscous inner wakes but were present in the outer wake as well. It is of interest to note that the region of complete cutoff for the present high speed, ablating aluminum models is on the order of 500 body diameters which compares with the length of the visible trail measured by Taylor et al. (Ref. 8).

Most of the models launched in support of this investigation have been photographed with a high-speed Fastax® camera which views the oncoming model for almost the total flight distance. A typical photograph of an ablating model is shown in Fig. 13. Solid, 0.125-in.-diam, copper spheres have been launched at similar flight conditions and the Fastax® camera records for these shots indicate only a small region of luminosity which can be associated with the model nose cap. Furthermore, for these flight conditions, i.e., a model velocity of 26,000 ft/sec and range pressure of 20 mm Hg, the wake of the copper sphere is transparent to the microwave energy (Fig. 9a).

4.3 WAKE VELOCITY MEASUREMENT

If the electron density in the wake of a body is sufficiently high, some of the incident microwave energy transmitted by the oblique radar will be reflected. The frequency of the backscattered signal can be related to the velocity of the regions of high electron density which gives rise to the reflection. Doppler radar data obtained from the turbulent wakes of high speed spheres have been interpreted in terms of apparent wake velocities. In calling such a velocity the wake velocity, it is assumed that the regions of high electron density are directly related to the overall fluid dynamic properties of the wake. In an earlier section it has been indicated that data from Ref. 6 imply that, for the velocities and pressures of the present investigation, the electron density in the wake of a nonablating sphere is too low to produce returns which can be detected by the present radar system. However, wake returns were recorded during some shots, and it has been shown that ablation appears as the most likely cause of the highly reflective wakes (cf. Fig. 3c). Using such data to determine wake properties is analogous to the experiments performed at Avco (Refs. 8 and 9) to delineate the extent and velocity of the turbulent wake by studying the luminosity generated by a highly ablating plastic model. The main concern in using the products of ablation to provide a source of reflection is to determine whether or not the fluid flow is modified to a significant extent. In Fig. 14 schlieren photographs of the turbulent wake of an ablating nylon sphere are shown. In Ref. 5 the variation of wake growth with axial distance behind this sphere has been compared to that of nonablating spheres and has been found to be the same (within the limitations of experimental accuracy). This would suggest that gross wake growth is not significantly affected by the degree of ablation associated with this model.

In Fig. 15 the axial velocity variation obtained with the 35-kmc focused oblique radar is compared with measurements made at MIT, Avco, and GM (Refs. 9 through 11) and also with the Lees-Hromas theoretical variation (Ref. 12). The present data are in fair agreement with these experimental and theoretical results. The radar data shown in Fig. 15 include wakes contaminated with five different materials: nylon, copper, aluminum, tungsten carbide, and steel. These five materials represent a range in specific gravity from approximately 1 to 15 and a melting temperature range from 500 to 3500°K. No consistent effect of material property on wake velocity can be detected. Therefore, it seems reasonable to assume that the measured wake velocities closely approximate the clean wake velocity which, in turn, contributes to the good agreement with the theoretical values.

It is of interest to note that the velocities measured by radar are greater than those measured with schlieren techniques, as shown in Fig. 15. The velocity measured with the oblique radar represents the local velocity at the particular portion of the wake from which the radar energy is reflected. (The clean wave form of the Doppler radar wake return, e. g. Fig. 3c, suggests that the reflection is from a uniform source.) Other radial stations in the wake, which have different velocities, may be transparent to or shielded from the microwave energy. Presumably it is these regions which affect the result obtained by schlieren usage and account for the discrepancy evident in Fig. 15. The good agreement between the measured luminous (Ref. 9) and radar wake velocities indicates that the contaminants which provide the source of luminosity and radar reflection are probably confined to the same region of the turbulent inner wake.

4.4 TRANSITION FROM LAMINAR TO TURBULENT FLOW

For the flight conditions of the present investigation, the sensitivity of the Doppler radar system is such that, as noted earlier, only reflections caused by the products of ablation generally can be detected. Because of the agreement between the radar-measured and theoretical values of turbulent wake velocity discussed in the previous section, it would seem reasonable to conclude that the products of ablation are confined to the inner viscous wake in that case. However, for the specularly-reflecting wakes behind ablating aluminum models, the products of ablation effectively shield the viscous and inviscid wakes for 500 body diameters, as discussed in an earlier section and illustrated in Fig. 12. For this reason it is not possible in this latter case to determine whether there is any large scale inner wake turbulence present. Furthermore, if the flow is turbulent for $x/d > 500$, experience has shown that the present system has not been able to detect turbulent wake returns that far behind a body.

For some small model sizes the scale of turbulence may be so small that it is below the sensitivity limit of a particular Doppler radar system, and the typical turbulent return will not be discernible. If the initial turbulent cell size is less than this minimum value, the first return from such a wake will occur further behind the body, at a position where this cell has grown to a detectable size. This means that for a particular frequency, true transition will only be detected if the initial turbulent cell size at transition is above the minimum detectable size.

It has been shown (Fig. 3a) that for a nonablating sphere the amplitude of the radar return from the model is symmetrical about the time

axis. If an ablating sphere has laminar flow immediately behind it, a low backscattered signal would be expected, followed by a turbulent return typified by the return shown in Fig. 16. The onsets of such disturbances have been interpreted as the inner wake transition points and have been determined for a range of models and flight conditions. These data are shown in Fig. 17. The transition data obtained from the nylon and aluminum models are in good agreement and indicate that the contaminant in each of these cases acts as a seedant and does not significantly modify the flow field. The present microwave measurements of transition distance for seeded wakes are in good agreement with the "clean wake" data obtained by General Motors (Ref. 10).

It has been suggested in Ref. 5 that the transition distance (as measured from schlieren photographs) in the wake of a sphere can be correlated in terms of the parameters $(V/\nu)_\infty x_{tr}/M_\infty$ and $(V/\nu)_\infty d$ for $(V/\nu)_\infty d \geq 10^5$. For high speeds, $M_\infty \approx 20$ and $(V/\nu)_\infty d \leq 10^5$, transition from laminar to turbulent flow in the inner viscous wake is difficult to detect with a schlieren system because the inviscid wake becomes a significant flow field observable (Fig. 7) and shields the inner viscous wake. It has been suggested in Ref. 5 and other references that for $(V/\nu)_\infty d \leq 10^5$ and $M_\infty \geq 20$, a schlieren system does not indicate transition from laminar to turbulent flow in the inner viscous wake but rather it indicates the point at which the turbulent inner viscous wake has broken through the inviscid wake (see sketch in Fig. 17). What are believed to be breakthrough distances obtained from the VKF and other schlieren results (Refs. 5 and 13) are shown in the upper part of Fig. 17. It will be noted in Fig. 17 that there is poor agreement between the schlieren measurement of distance to breakthrough and the microwave-measured transition distance in the inner viscous wake, which is consistent with the above argument.

From the foregoing discussion it seems reasonable to conclude that a 35-kmc oblique Doppler radar system can detect transition in the inner viscous wake provided this wake will reflect the incident microwave energy and is not shielded by the products of ablation as discussed in an earlier section. On the strength of these data, this apparent paradox cannot be fully explained. From Fig. 10, it is noted that the shot conditions represented in Fig. 12, where sufficient electron density existed all the way to the shock boundaries to cutoff transmission, are characterized by one to ten times greater (nonablating) electron production than the shots of Fig. 15, where it is implied that the significant electron density was confined to the inner wake. However, this difference does not seem conclusive, and it only can be said that in some lower pressure, high speed cases (Fig. 12) the inner wake is hidden by an apparent over-density of electrons in the entire flow field. The dividing line between these two different situations is not defined as yet.

SECTION V
CONCLUSIONS

The present radar experiments indicate that detectable reflections obtained from the wakes of hypervelocity spheres by the 35-kmc equipment described herein were closely related to, and probably solely originated from, sphere ablation. The ablation-induced radar signature of the wake is characterized by the laminar or turbulent nature of the wake. The laminar wake of an ablating sphere produces a very low frequency radar return and reflects the microwave energy at a 90-deg angle to the incident radar beam when the angle of incidence is 45 deg. The radar signal from the turbulent wake of an ablating sphere displays a higher frequency and indicates a wake velocity that agrees reasonably well with theoretical calculations and other experimental results. Radar measurements of the transition distance agree with other radar results and also with schlieren-measured distances.

REFERENCES

1. Bailey, A. B. "Sphere Drag Measurements in an Aeroballistic Range at High Velocities and Low Reynolds Numbers." AEDC-TR-66-159, May 1966.

2. Carswell, A. I. and Richard, C. "Focused Microwave Systems for Plasma Diagnostics." RCA Victor Research Report No. 7-801-32, December 1964.

3. Hidalgo, H., Taylor, R. L., and Keck, J. C. "Transition in the Viscous Wake of Blunt Bodies at Hypersonic Speeds." Avco Everett Research Laboratory, Research Report 133, April 1961.

4. Kornegay, Wade M. "Electron Density Decay in Wakes." AIAA Journal, Vol. 3, No. 10, October 1965, pp. 1819-1823.

5. Bailey, A. B. "Turbulent Wake and Shock Shape of Hypervelocity Spheres." AEDC-TR-66-32 (AD484821), July 1966.

6. Eschenroeder, A. Q., Hayami, R., Primich, R., and Chen, T. "Ionization in the Near Wakes of Spheres in Hypersonic Flight." AIAA 3rd Aerospace Sciences Meeting, New York, January 24-26, 1966, AIAA Paper No. 66-55.

7. Heald, M. A. and Wharton, C. B. Plasma Diagnostics with Microwaves. John Wiley and Sons, Inc., New York, 1965.

8. Taylor, R. L., Melcher, B. W., II, and Washburn, W. K. "Measurements of the Growth and Symmetry of the Luminous Hypersonic Wake behind Blunt Bodies." Avco-Everett Research Laboratory Research Report No. 163-BSD TDR-63-108, May 1963.

9. Hidalgo, H., Taylor, R. L., and Keck, J. C. "Transition in the Viscous Wake of Blunt-Bodies at Hypersonic Speeds." Avco-Everett Research Laboratory, Research Report 133, April 1961.

10. Primich, R. I., Robillard, P. E., Eschenroeder, A. Q., Wilson, L., and Zivanovic, S. "Radar Scattering from Wakes." General Motors Corporation TR-65-01E, March 1965.

11. Slattery, R. E. and Clay, W. G. "The Turbulent Wake of Hypersonic Bodies." American Rocket Society 17th Annual Meeting and Space Flight Exposition, Nov. 13-18, 1962, No. 2673-62.

12. Lees, Lester and Hromas, Leslie. "Turbulent Diffusion in the Wake of a Blunt-Nosed Body at Hypersonic Speeds." Journal of Aerospace Sciences, Vol. 23, No. 8, August 1962, pp. 976-993.

13. Clay, W. G., Labitt, M., and Slattery, R. E. "Measured Transition from Laminar to Turbulent Flow and Subsequent Growth of Turbulent Wakes." AIAA Journal, Vol. 3, No. 5, May 1965, pp. 837-841.

29

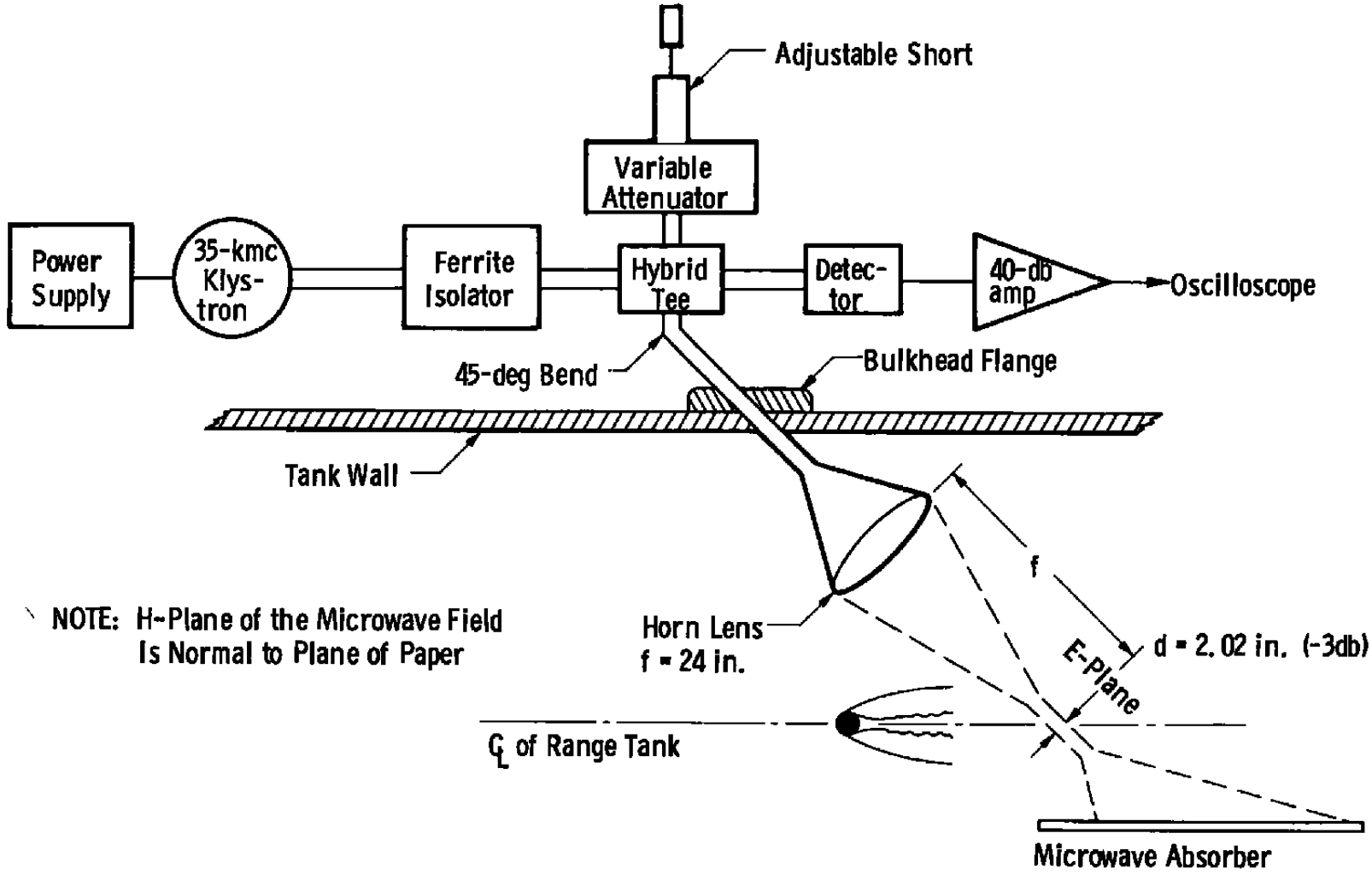

Fig. 1 35-kmc Oblique Doppler Radar System

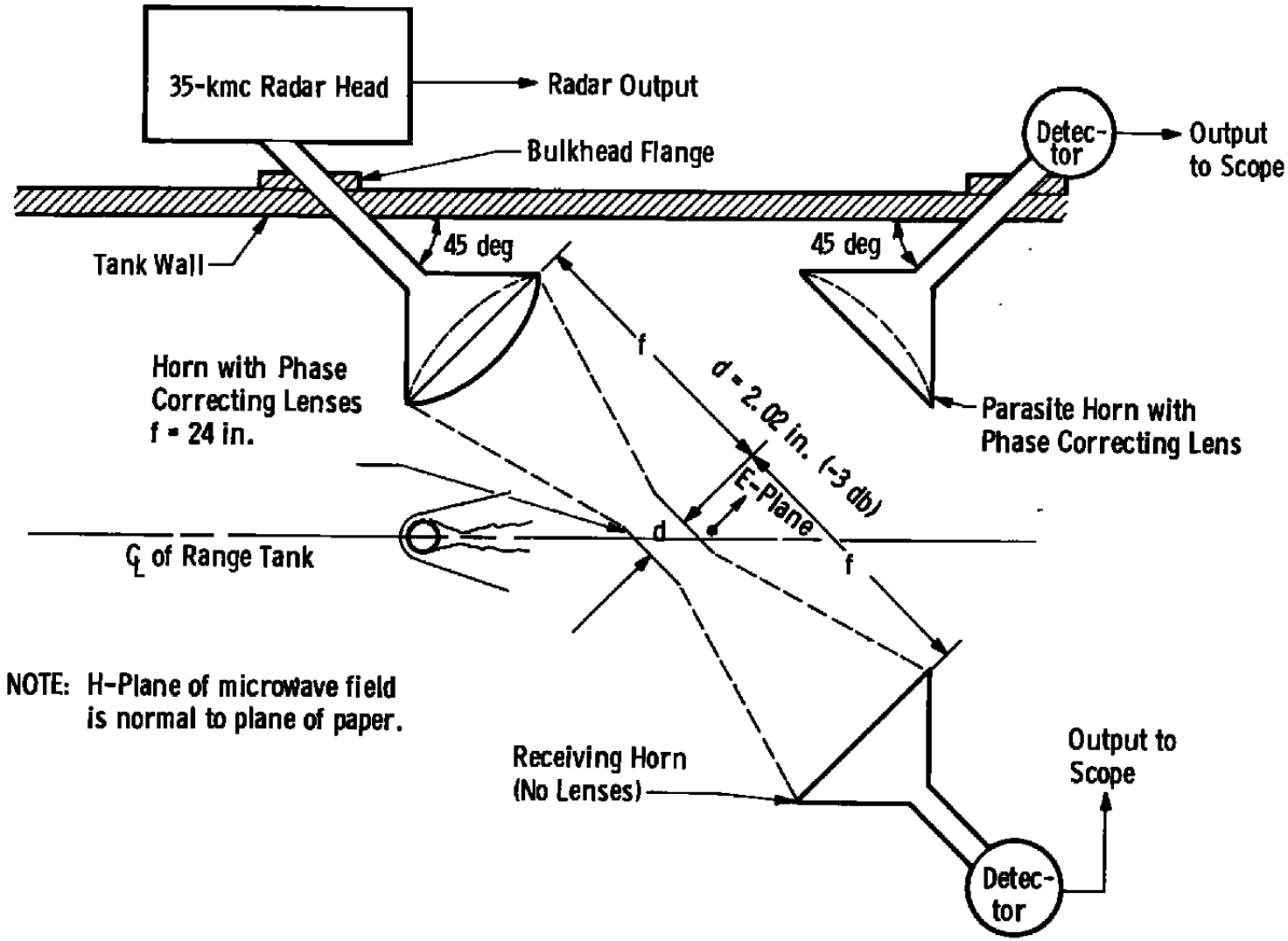

Fig. 2 35-kmc Oblique Doppler Radar System – Receiving and Parasite Antennas

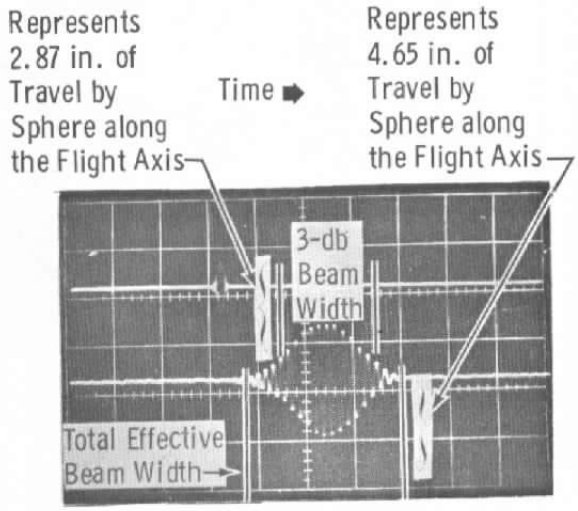

Vertical Sensitivity = 1 v/cm
Horizontal Sensitivity = 100 μsec/cm

Delayed Sweep

Vertical Sensitivity = 500 mv/cm
Horizontal Sensitivity = 10 μsec/cm

a. Shot K-1318
0.437-in.-diam Aluminum Sphere
Model Velocity = 11,400 ft/sec
Range Pressure = 25 mm Hg

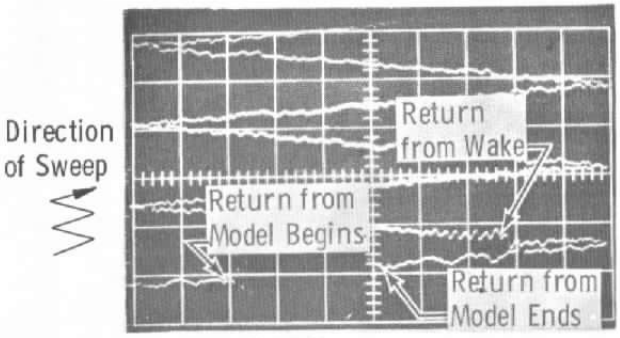

Vertical Sensitivity = 200 mv/cm
Horizontal Sensitivity = 10 μsec/cm

b. Shot K-1347
0.375-in.-diam Nylon Sphere
Model Velocity = 10,500 ft/sec
Range Pressure = 99 mm Hg
Blast Tank Pressure = 600 mm Hg

Fig. 3 Typical Records from Oblique (45-deg) Doppler Radar

Time ➡

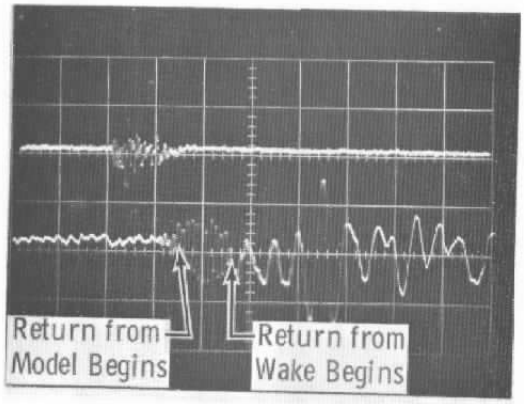

Vertical Sensitivity = 200 mv/cm
Horizontal Sensitivity = 100 μsec/cm

Delayed Sweep

Vertical Sensitivity = 100 mv/cm
Horizontal Sensitivity = 10 μsec/cm

c. Shot K-1316
0.125-in.-diam Steel Sphere
Model Velocity = 17,700 ft/sec
Range Pressure = 200 mm Hg

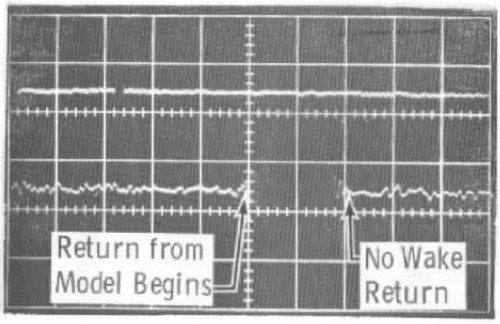

Vertical Sensitivity = 200 mv/cm
Horizontal Sensitivity = 100 μsec/cm

Delayed Sweep

Vertical Sensitivity = 100 mv/cm
Horizontal Sensitivity = 10 μsec/cm

d. Shot K-1313
0.125-in.-diam Tungsten-Carbide
Model Velocity = 19,400 ft/sec
Range Pressure = 200 mm Hg

Fig. 3 Concluded

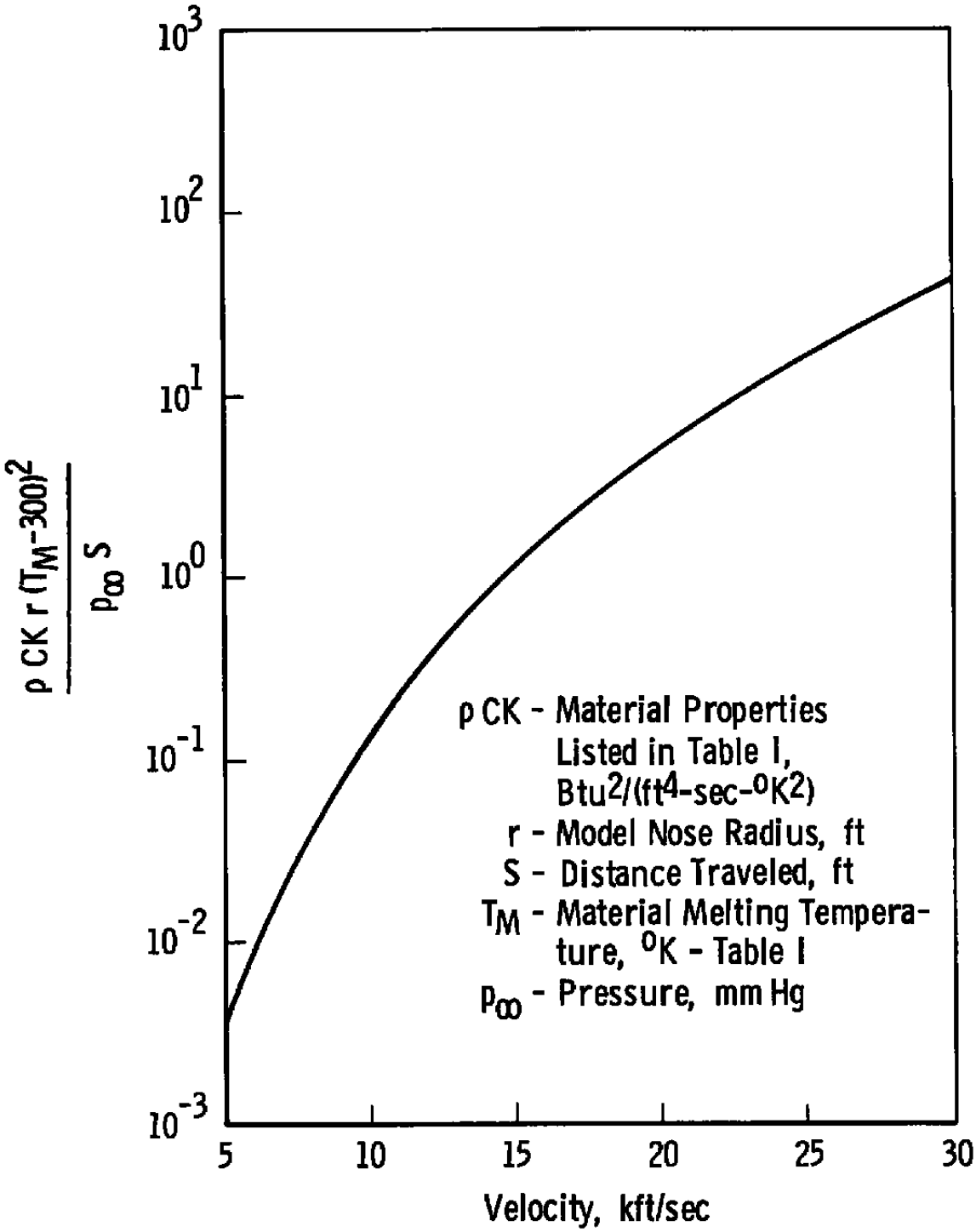

Fig. 4 Flight Conditions which Will Give Material Melting Temperature at the Stagnation Point

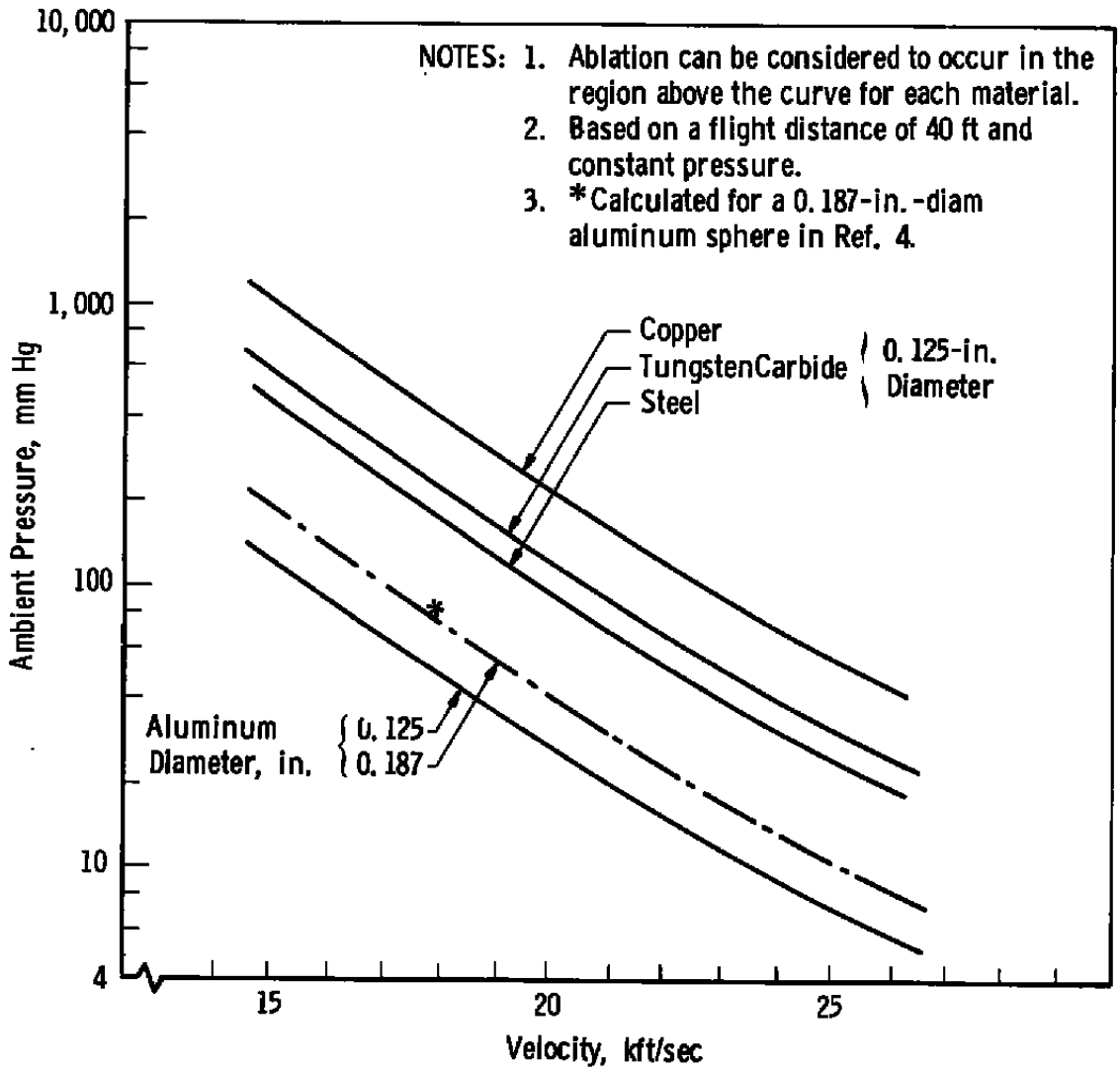

Fig. 5 Calculated Melting Temperature Boundaries

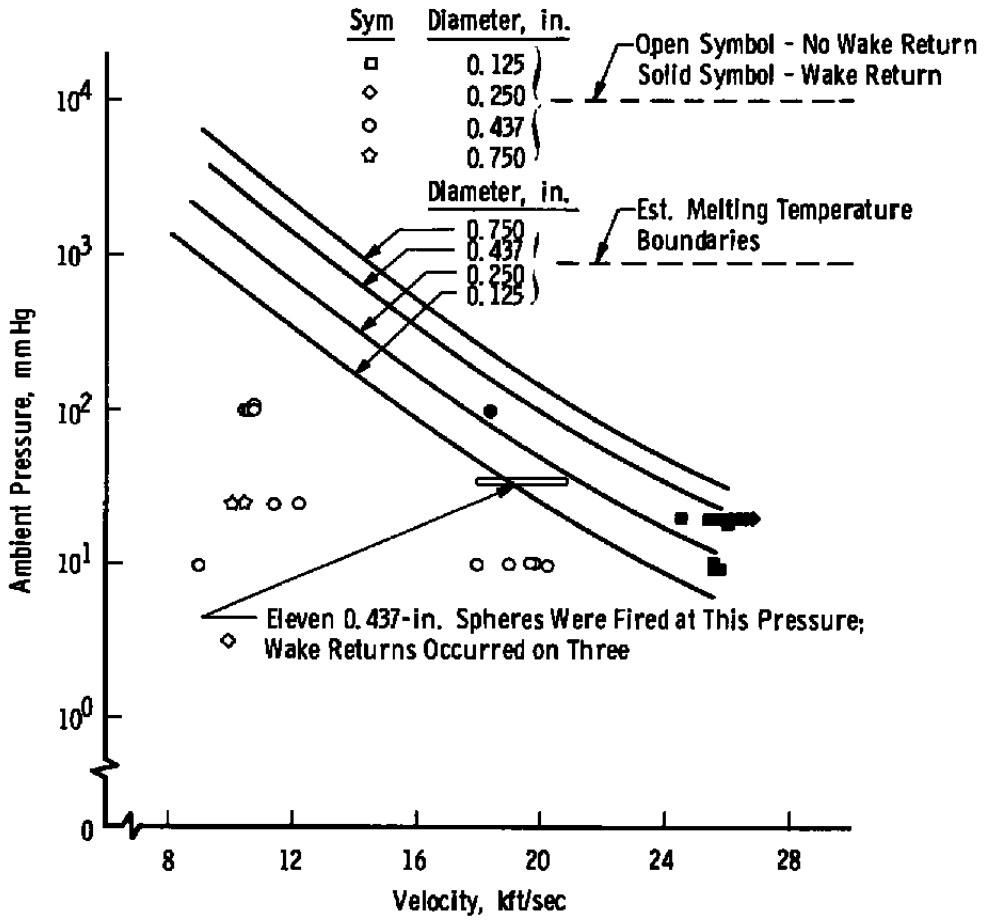

a. Aluminum Spheres

Fig. 6 Comparison of Radar Wake Returns with Predicted Ablation

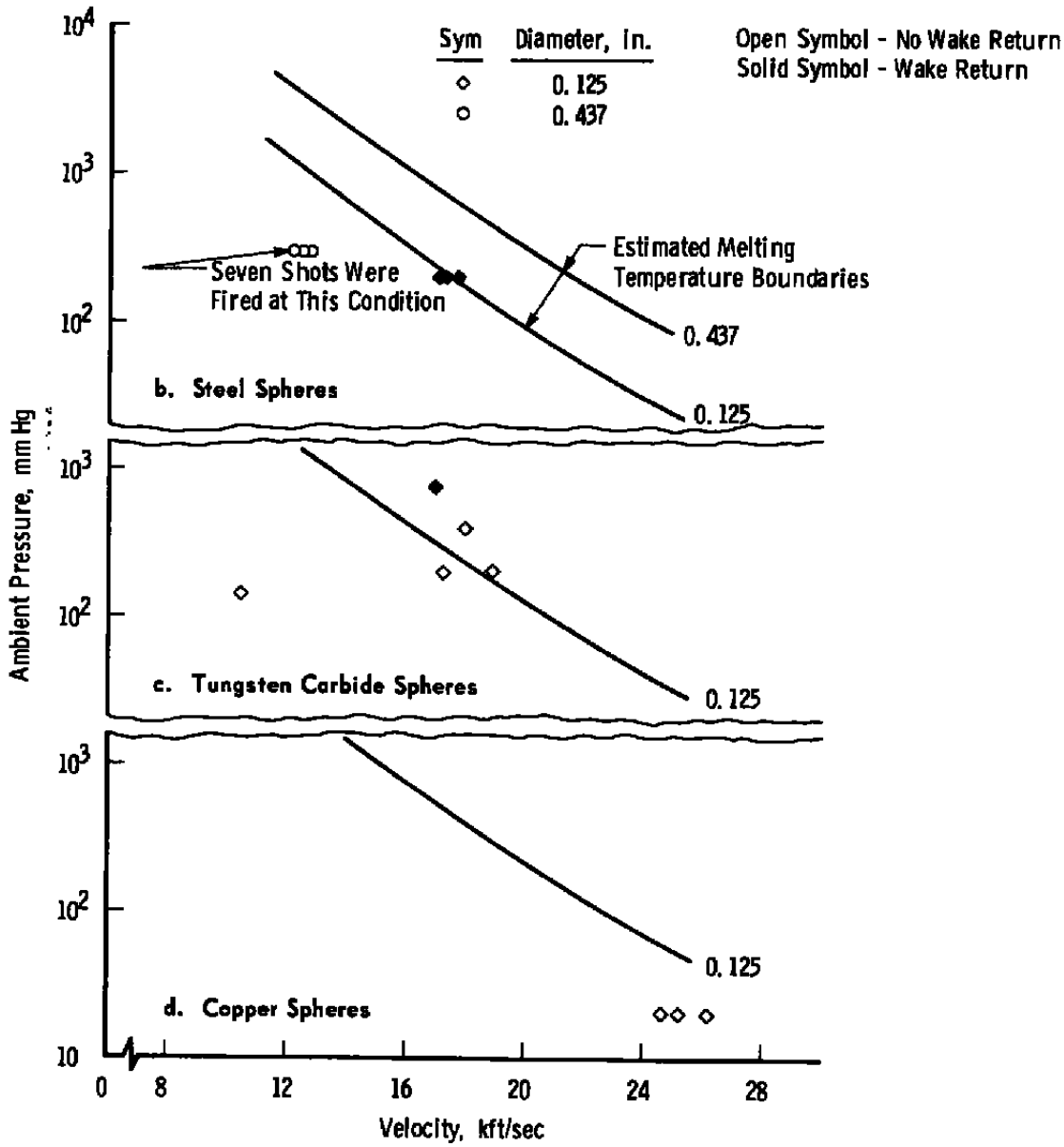

Fig. 6 Concluded

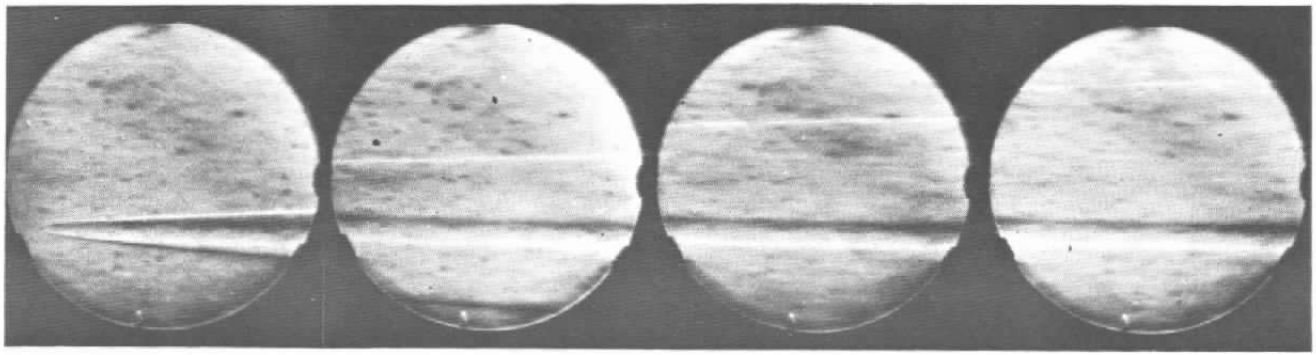

430 680 930

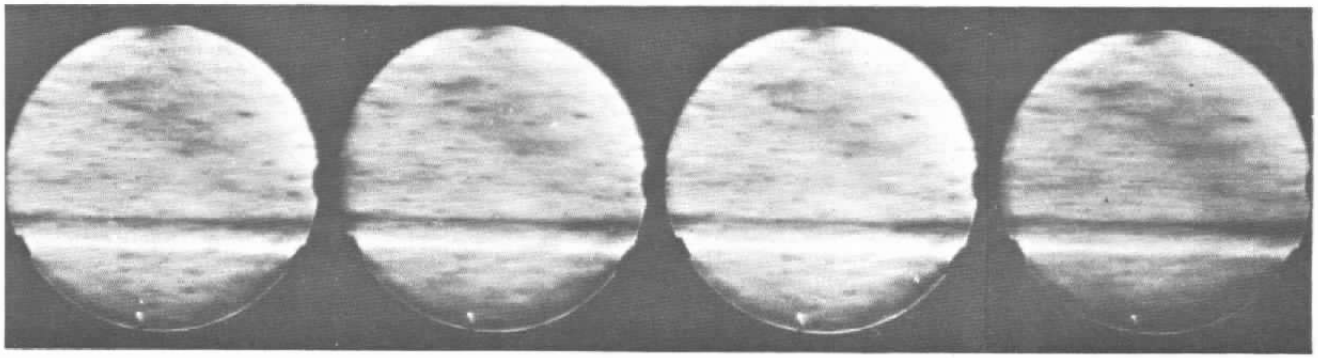

3430 3680 3930 4180

Axial Distance from Center of Picture to the Model in Body Diameters

Shot No. 1418
V_∞ = 26, 200 ft/sec
p_∞ = 19. 6 mm Hg
0. 125-in. -diam
Copper Sphere

Fig. 7 Laminar Wake behind a High Speed Sphere

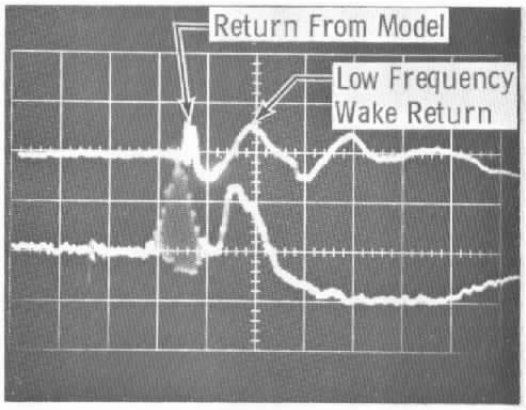

Vertical Sensitivity = 500 mv/cm
Horizontal Sensitivity = 100 μsec/cm

Delayed Sweep

Vertical Sensitivity = 200 mv/cm
Horizontal Sensitivity = 10 μsec/cm

a. Oblique Radar Record

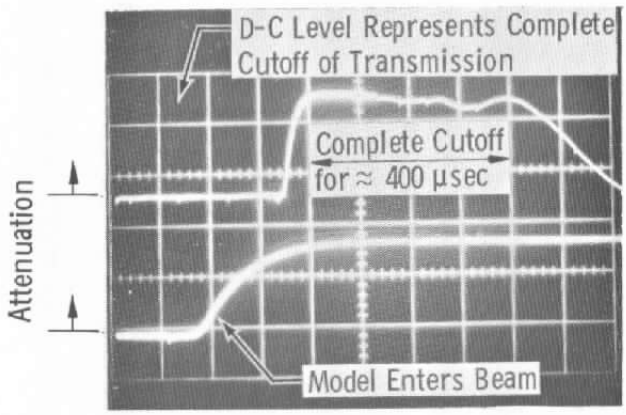

Vertical Sensitivity = 200 mv/cm
Horizontal Sensitivity = 100 μsec/cm

Delayed Sweep

Vertical Sensitivity = 200 mv/cm
Horizontal Sensitivity = 20 μsec/cm

b. Transmission

Shot K-1408
0.25-in.-diam Aluminum Sphere
Model Velocity = 26,200 ft/sec
Range Pressure = 19.8 mm Hg

Fig. 8 Radar, Receiving, and Parasite Antenna Records Illustrating Complete Cutoff

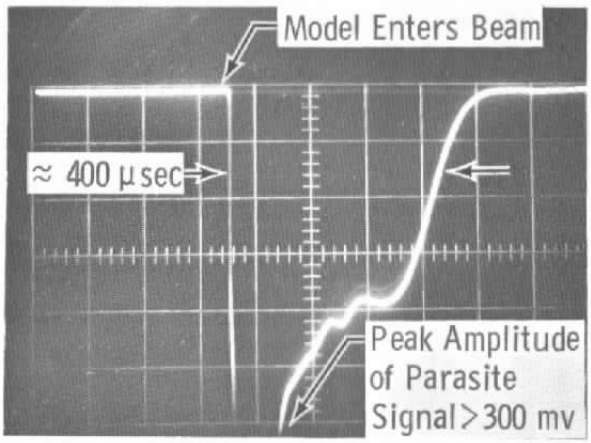

Vertical Sensitivity = 50 mv/cm
Horizontal Sensitivity = 100 µsec/cm

Shot K-1415
0.25-in.-diam Aluminum Sphere
Model Velocity = 25,800 ft/sec
Range Pressure = 18.9 mm Hg

c. Parasite Antenna Signal

Fig. 8 Concluded

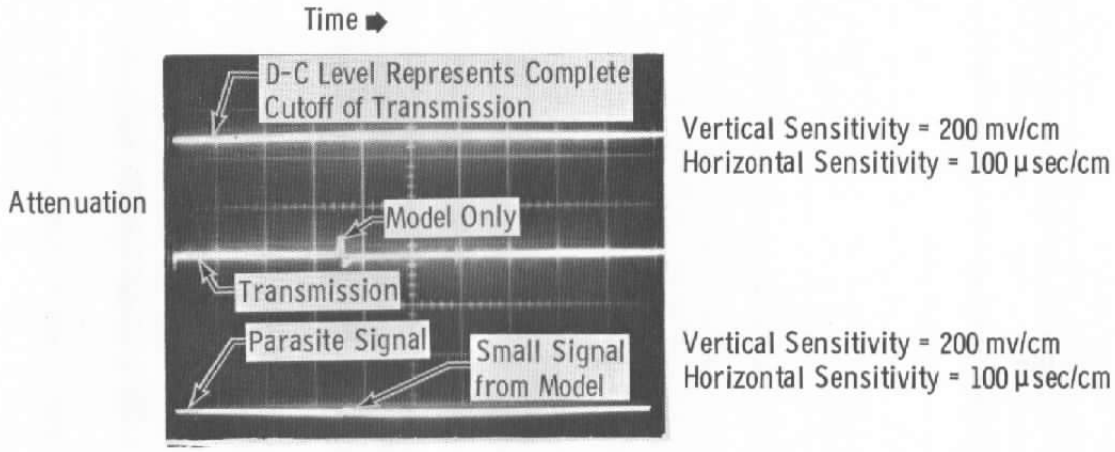

a. Shot K-1420
0.125-in.-diam Copper Sphere
Model Velocity = 25,200 ft/sec
Range Pressure = 19.8 mm Hg

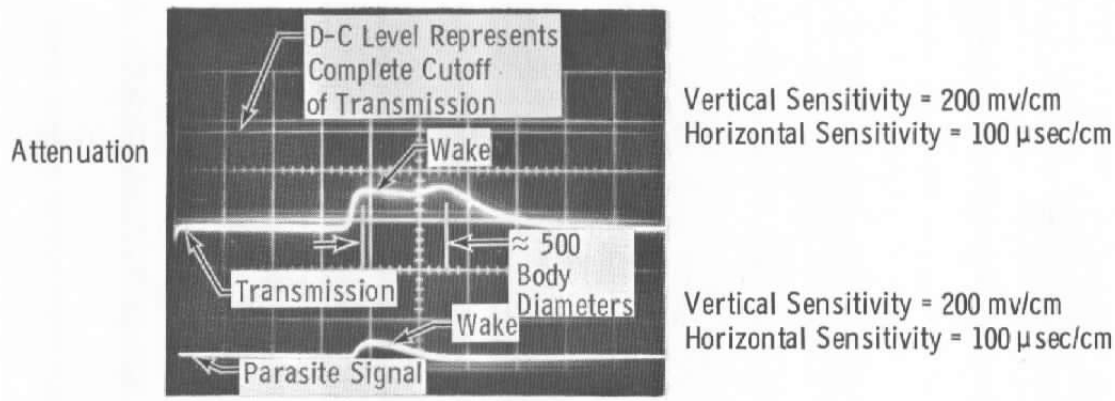

b. Shot K-1425
0.125-in.-diam Aluminum Sphere
Model Velocity = 26,700 ft/sec
Range Pressure = 20 mm Hg

Fig. 9 Receiving and Parasite Antenna Records from 0.125-in.-diam Metal Spheres

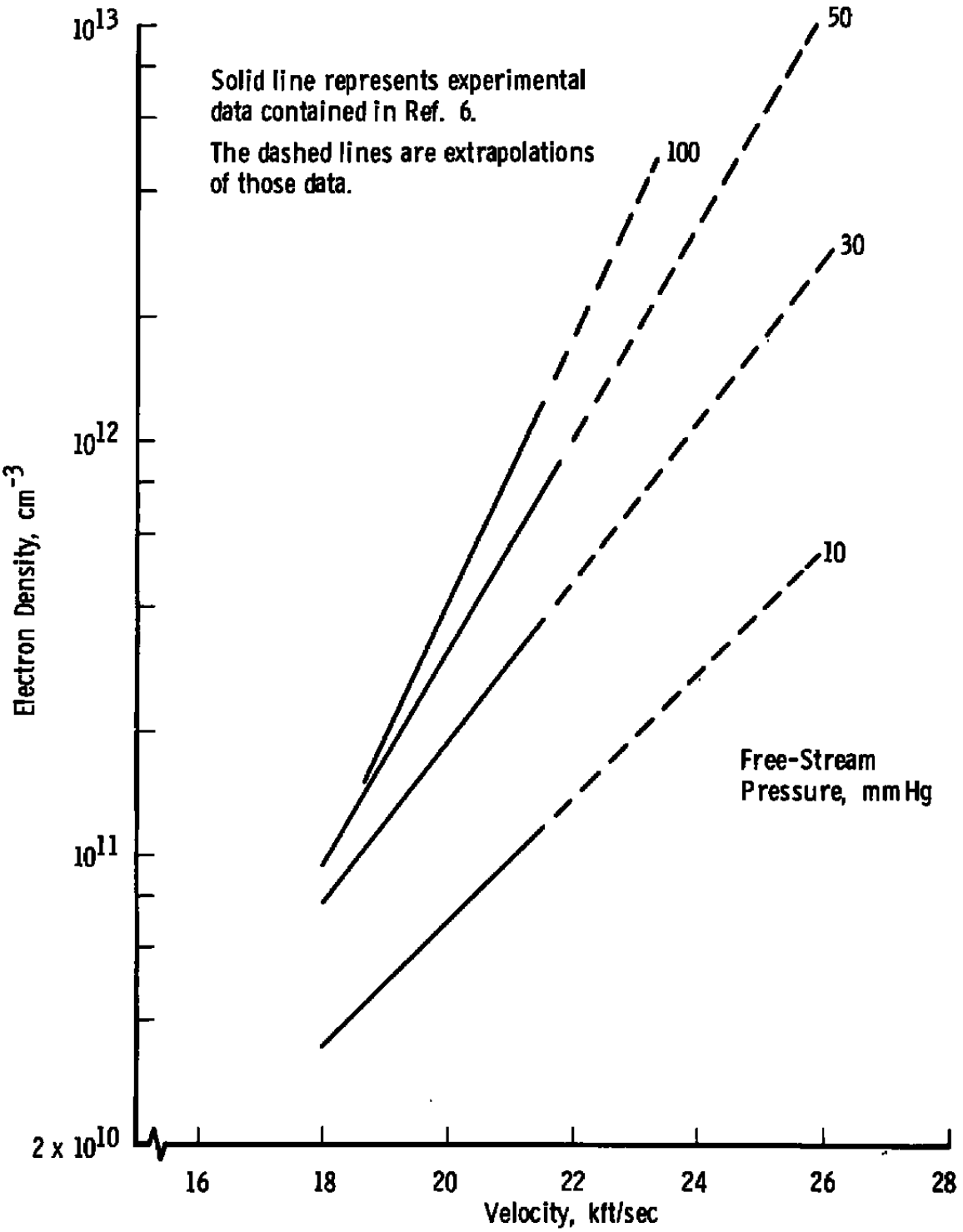

Fig. 10 Variation of Electron Density with Velocity and Ambient Pressure for a Sphere for x/d = 40

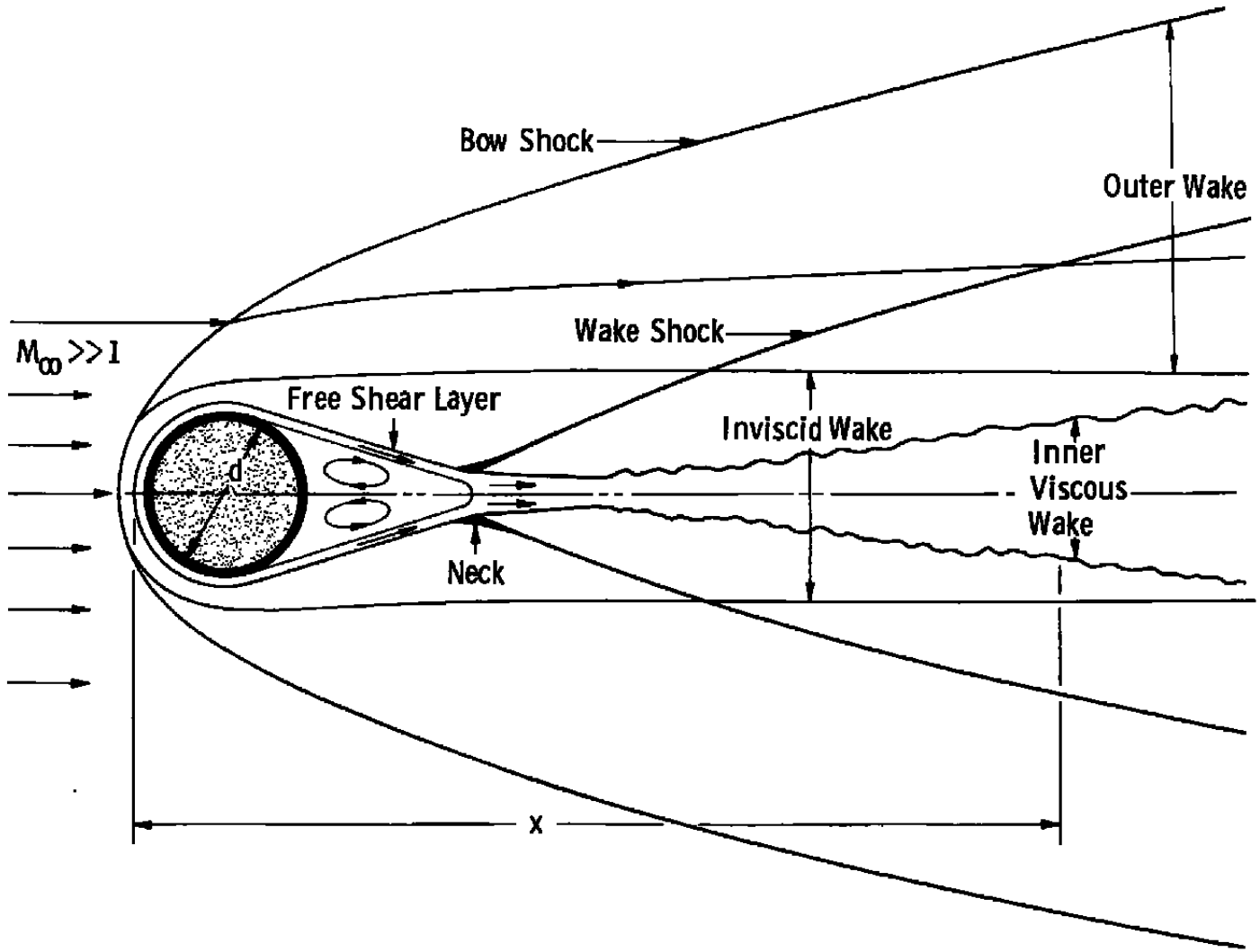

Fig. 11 Wake behind a Blunt Body at Hypersonic Speeds

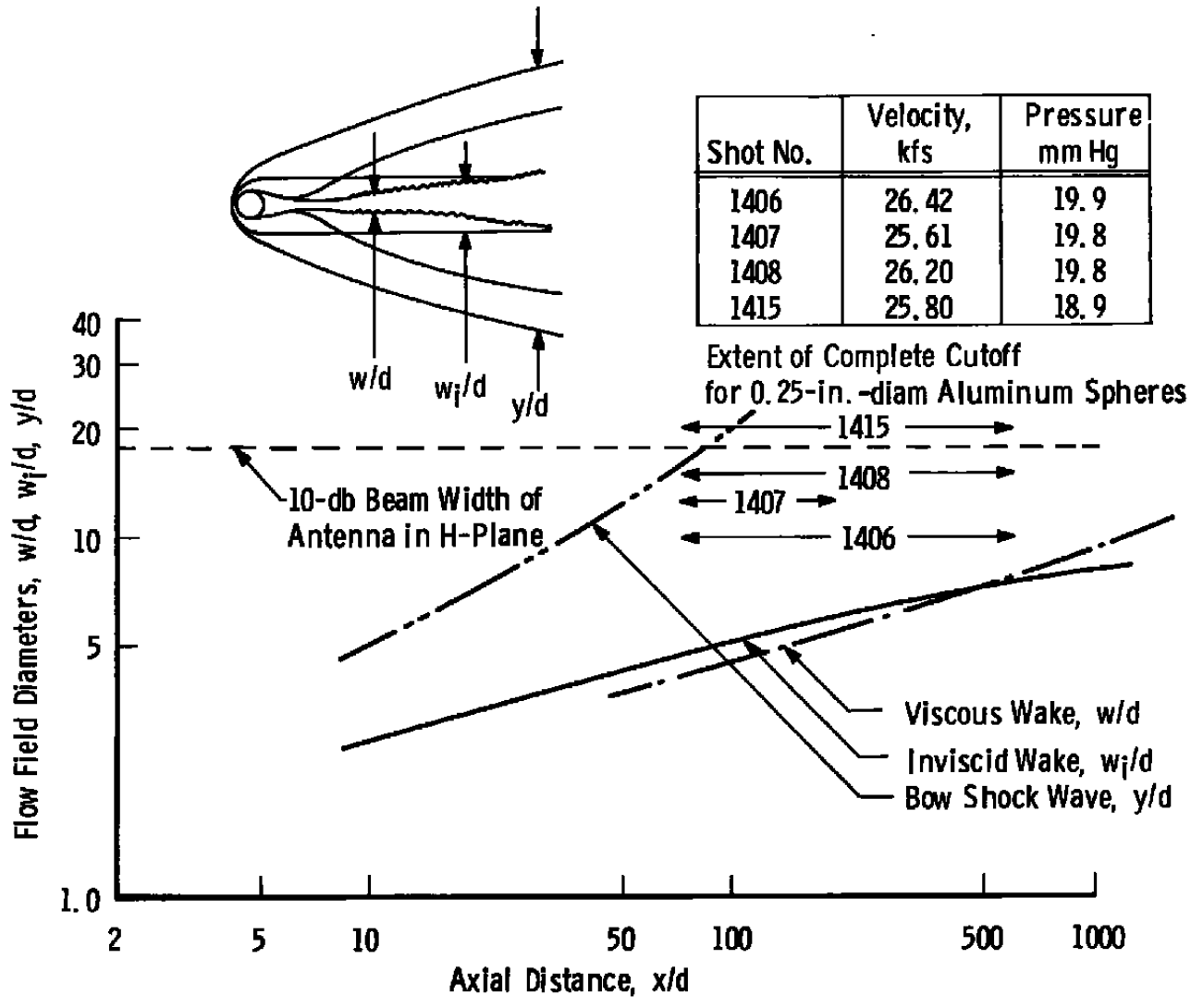

Fig. 12 Shock Shape and Viscous and Inviscid Wake Diameters for a High Speed Sphere

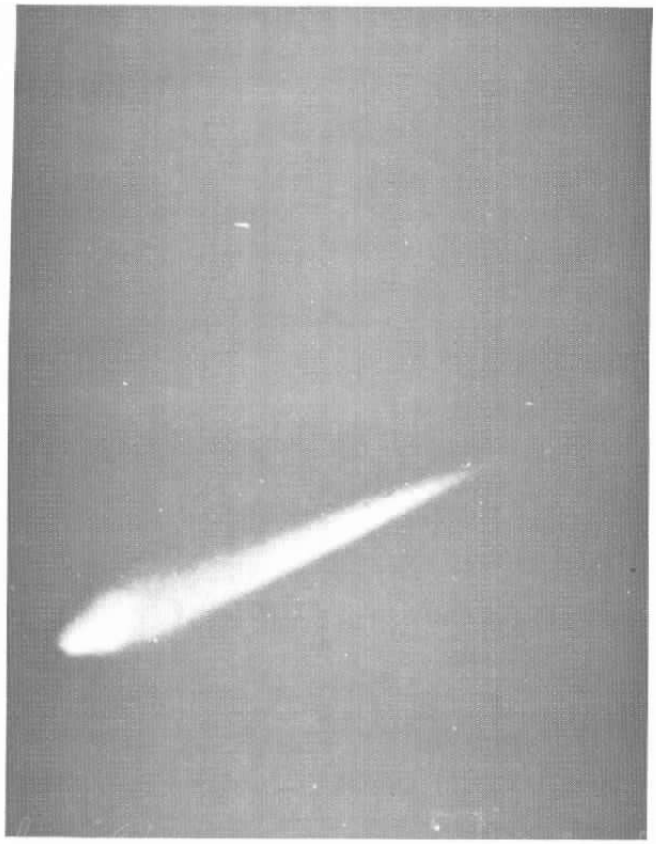

Shot K-1388
0.25-in.-diam Aluminum Sphere
Model Velocity = 26,000 ft/sec
Range Pressure = 9.8 mm Hg

Fig. 13 Fastax® Photograph of an Ablating Model and Wake

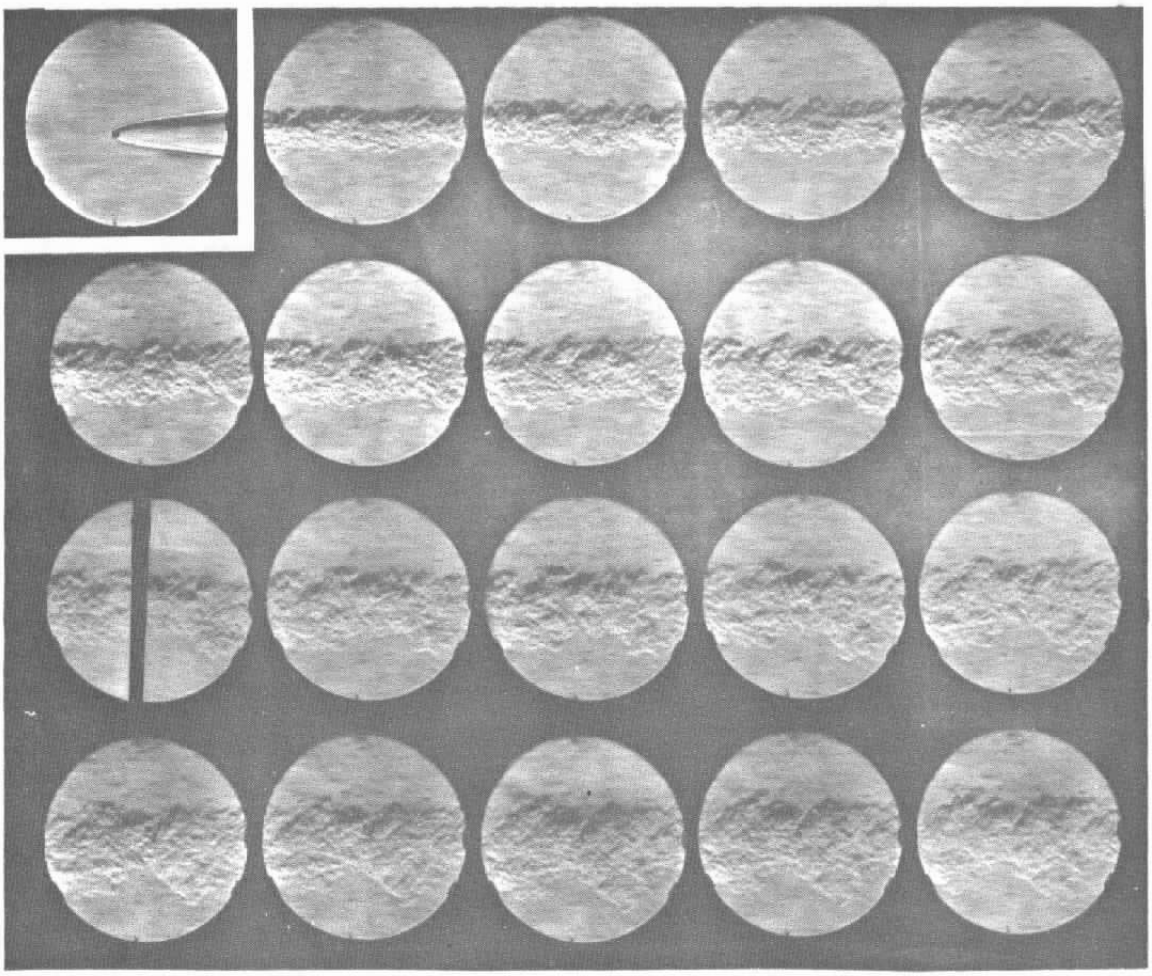

Range K Shot 1372
1/4-in.-diam Nylon Sphere
Frame Spacing is 470
Body Diameters
V_∞ = 20,650 ft/sec
p_∞ = 50 mm Hg

Fig. 14 Turbulent Far Wake of an Ablating Sphere

Sym	V_∞, kfps	P_∞, mm Hg	Material	Diameter, in.	Source
Oblique Focused Doppler Radar					
☆	15.6-21.0	35	Aluminum	0.25-0.437	VKF
★	17.4-18.5	200	Steel	0.125	↓
●	20.5	50	Nylon	0.25	↓
◆	17.0	734	Tungsten Carbide	0.125	↓
——·——	17.6-19.6	50-100	Copper	0.2 -0.6	Ref. 10
Schlieren					
△	10.0-11.0	100	Aluminum	0.437	VKF
– – – –	7.6	≈760	Aluminum	0.50	Ref. 11
Luminosity-Drum Camera Technique					
——– ——	13.5-14.0	40-60	Lexan	0.55	Ref. 9

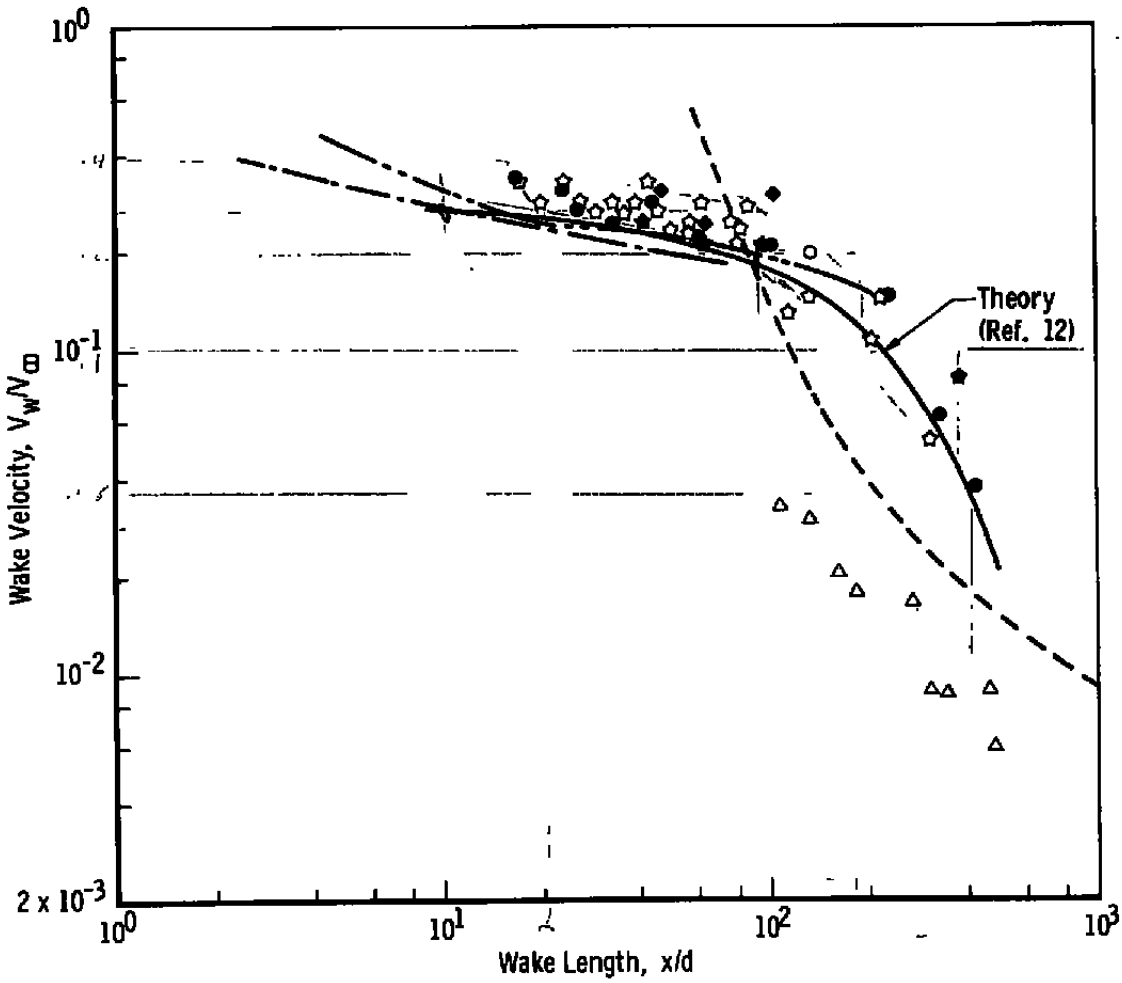

Fig. 15 Wake Velocity behind a Sphere

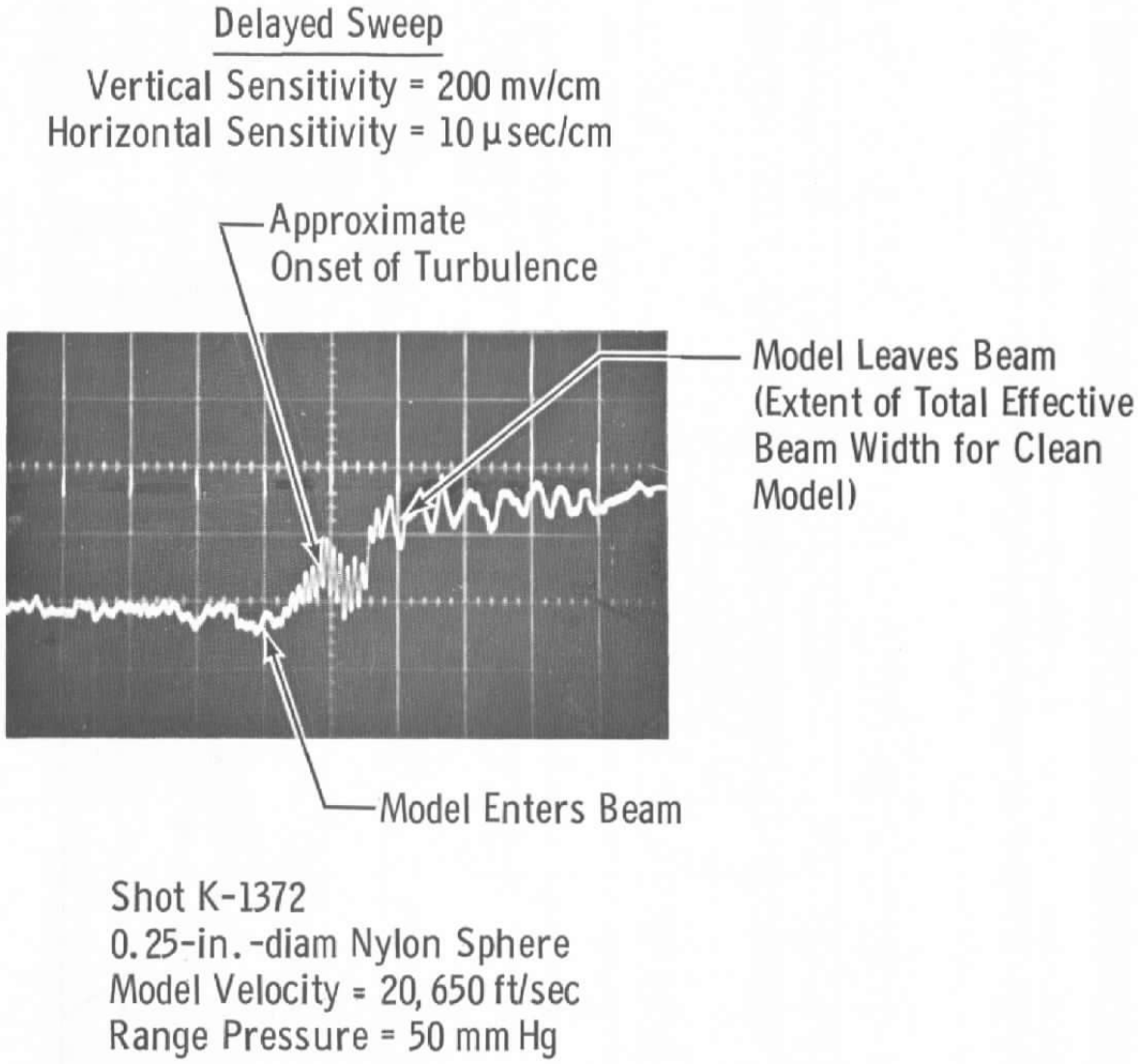

Fig. 16 Transition from Laminar to Turbulent Flow

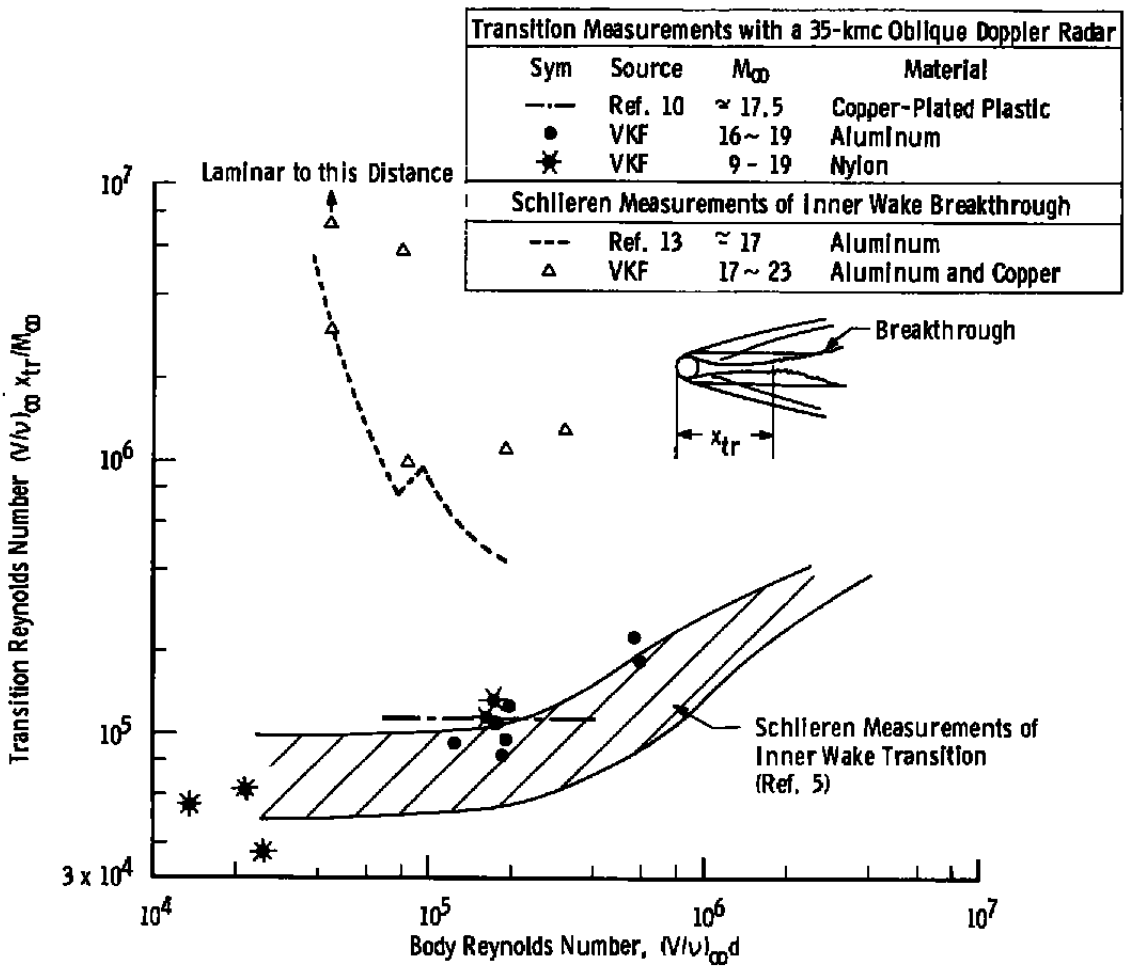

Fig. 17 Comparison of Schlieren and Microwave Measured Transition Distance

TABLE I
MATERIAL PROPERTIES

Material	Density, ρ, lb/ft^3		Thermal Conductivity, K-Btu/sec/ft^2/°K/ft		Specific Heat, C, Btu/lb/°K		ρCK, Btu^2/ft^4-$°K^2$-sec		Melting Temperature, T_M, °K	
	High	Low	High	Low	High	Low	High	Low	High	Low
Aluminum*	185	160	0.068	0.026	0.415	0.396	5.21	1.65	930	761
Beryllium	115	--	0.043		0.810	--	3.99	--	1555	--
Copper	559	555	0.113	0.098	0.180	0.162	11.36	8.81	1355	1337
Glass	268	156	0.001	0.00025	0.360	0.288	0.096	0.011	1955	855
Gold	1204	--	0.086	-	0.056	--	5.80	--	1336	--
Magnesium*	110	105	0.040	0.012	0.441	--	1.94	0.556	923	717
Polycarbonate†	94	75	0.00005	0.000025	0.540	--	0.003	0.001	558†	--
Silver	655	--	0.119	--	0.101	--	7.87	--	1235	--
Steel*	501	464	0.019	0.004	0.252	0.162	2.40	0.30	1813	1645
Titanium	295	276	0.005	0.002	0.234	0.216	0.34	0.12	1945	1775
Tungsten	1211	--	0.048	--	0.061	--	3.56	--	3690	--
Tungsten Carbide	976	--	0.0125	--	0.090	--	1.10	--	3140	--
Fansteel 60	1050	--	0.0225	--	0.086	--	2.04	--	3300	--

*Includes Alloys

†Melting Point (Crystalline)

‡Typical sabot material. More detailed information is given in "Materials in Design Engineering - Materials Selector Issue." Reinhold Publishing Corporation, October 1964.

TABLE II
STUDY OF SPHERE WAKES – 35-KMC OBLIQUE RADAR
(January 1965 to 1966 – Range K)

Shot No.	Velocity*, ft/sec	Range Pressure†, mm Hg	Model Material	Model Diameter, in.	y**, in.	Radar Return Model	Radar Return Wake	Transmission	Remarks
1067	19,190	34.7	Aluminum	0.437	-0.486	Yes	No	Not recorded	Spurious signals began ~ 5 ft behind model
1068	19,350	34.9			-0.824		No		Spurious signals began ~ 5 ft behind model
1069	20,540	34.2			-0.627		No		Spurious signals began ~ 8 ft behind model
1071	19,300	34.9			-0.383		Yes		Wake return began immediately behind model and lasted 15 μsec
1076	19,400	34.7			0.06		No		No wake return
1077	19,200	34.7			-0.062		Yes		Wake return began immediately behind model and lasted 130 μsec
1078	19,500	34.9			-0.12		No		No wake return
1079	19,300	35.4			-0.15		No		No wake return
1080	18,750	34.9			-0.507		Yes		Wake return began immediately behind model and lasted 20 μsec
1081	18,400	34.6			-0.556		No		No wake return
1082	18,070	35.0			-0.049		No		No wake return
1083	12,500	300.0	Steel		-0.46		No		Large model return
1084	12,200	300.0			-0.614		No		
1086	12,500	300.0			-0.34		No		
1087	12,550	300.0			-0.69		No		
1088	12,700	299.0			-0.61		No		
1090	12,280	300.0			-0.29		No		
1091	12,200	299.0			-0.29		No		

TABLE II (Continued)

Shot No.	Velocity*, ft/sec	Range Pressure, mm Hg	Material	Model Diameter, in.	y**, in.	Radar Return Model	Radar Return Wake	Transmission	Remarks
1243	10,000	25.0	Aluminum	0.75	0.60	Yes	No	Not recorded	Large model return
1244	10,200	25.0	Aluminum	0.75	-0.25		No		
1248	9,900	3.1	Aluminum	0.125	-0.83		No		
1252	10,580	150.0	W/C	0.125	-1.23		No		
1270	10,570	100.0	Aluminum	0.437	0.45		No		
1272	10,620	100.0		0.437	0.39		No		
1273	10,750	100.0		0.437	0.31		No		
1274	10,520	100.0		0.437	-1.14		No		
1309	17,320	200.0	Steel	0.125	-1.09		Yes		Large return from model and wake lasting ≈100 μsec
1310	18,900	200.0	W/C	0.125	0.9		No		No wake return
1312	17,200	200.0	Steel	0.125	-1.06		Yes		Large return from model and wake
1313	17,220	200.0	W/C	0.125	-1.15		No		No wake return
1316	17,700▲	200.0	Steel	0.125	No data		Yes		Large return from model and wake
1318	11,400	25.0	Aluminum	0.437	-1.13		No		Large model return
1319	12,170	25.0	Aluminum	0.437	-0.64		No		Large model return
1322	17,000	734.0	W/C	0.125	No data		Yes		Large return from model and wake
1324	18,030	400.0	W/C	0.125	1.07		No		No wake return
1344	9,000	9.9	Aluminum	0.437	-0.32		No	Attenuation by model	No wake return
1346	10,200	10(610)‡	Nylon	0.375	-0.25		Yes	Attenuation	Small model and wake return; attenuation by model and wake

TABLE II (Continued)

Shot No.	Velocity*, ft/sec	Range Pressure, mm Hg	Material	Model Diameter, in.	y**, in.	Radar Return Model	Radar Return Wake	Transmission	Remarks
1347	10,500	99(600)‡	Nylon	0.375	-0.35	Yes	Yes	Attenuation	Small model and wake return, attenuation by model and wake
1351	20,230	9.9	Aluminum	0.437	-0.62		No	Attenuation by model	Small low frequency wake signal
1352	18,300	100.0	Aluminum	0.437	No data		Yes	Attenuation	Large return from model and wake; corresponding attenuation by model and wake
1354	19,000	10.2	Aluminum	0.437	-0.89		No	Attenuation	Small low frequency wake signal; slight attenuation by wake
1360	20,200	50.0	Nylon	0.25	0.17	No	No	Amplification	No radar return, only low frequency shift; receiver horn showed apparent gain for ≈1 msec
1363	19,100	50.0	Nylon	0.25	-0.27	No	No	Amplification	No radar return, only low frequency shift; receiver horn showed apparent gain for ≈1 msec
1372	20,650	50.0	Nylon	0.25		Yes	Yes	Attenuation	Model and wake return
1373	19,000	10.0	Aluminum	0.437	-0.35	Yes	No	Attenuation by model	Small low frequency wake signal
1374	17,870	10.0	Aluminum	0.437	-0.67	Yes	No		
1375	19,730	10.0	Aluminum	0.437	-0.38	Yes	No		
1376	19,650	10.0	Aluminum	0.437	-0.12	Yes	No		
1378	18,800	50.0	Nylon	0.25	-0.13	Yes	Yes	Amplification by wake	Large return from model and wake, attenuation by model and gain from wake
1392	25,500	8.8	Aluminum	0.25	No data	No data		Attenuation by model and wake	No radar data recorded; attenuation by model and wake

TABLE II (Continued)

Shot No.	Velocity*, ft/sec	Range Pressure, mm Hg	Material	Model Diameter, in.	y**, in.	Radar Return Model	Radar Return Wake	Transmission	Remarks
1399	25,800	9.2	Aluminum	0.25	0.58	Yes	No	Attenuation by model and wake	No wake return; only slight shift, attenuation by model and wake
1402	25,320	9.4		0.25	0.46	No data			No radar data recorded; attenuation by model and wake
1404	25,500	10.2		0.25	0.28	Yes	No		No wake return, only slight shift, attenuation by model and wake
1406	26,420	19.9		0.25	0.26	Yes	Yes	Cutoff attenuation	A low frequency wake signal; complete cutoff of transmission for ~400 μsec
1407	25,610	19.8		0.25	-0.37	Yes	Yes	Cutoff attenuation	A low frequency wake signal, complete cutoff of transmission for ~200 μsec
1408	26,200	19.8		0.25	-0.37	Yes	Yes	Cutoff attenuation	A low frequency wake signal, complete cutoff of transmission for ~400 μsec
1409	25,800	19.9		0.25	No data	No	No	Small gain from wake	Small signal received by parasite horn; model passed through edge of beam
1414	24,530	19.5		0.25	0.27	Yes	Yes	Small attenuation by wake	Small signal from parasite horn and small attenuation by wake
1415	25,800	18.9		0.25	0.15	Yes	Yes	Cutoff attenuation	Low frequency wake signal; complete cutoff of transmission for ~400 μsec; large signal from parasite horn

TABLE II (Concluded)

Shot No.	Velocity*, ft/sec	Range Pressure, mm Hg	Material	Model Diameter, in.	y**, in.	Radar Return Model	Radar Return Wake	Transmission	Remarks
1420	25,200	19.8	Copper	0.125	0.68	Yes	No	Attenuation by model	No wake return; no signal from parasite horn
1423	24,600	20.0	Copper	0.125	0.18	Yes	No	Attenuation by model	No wake return, no signal from parasite horn
1424	26,600	20.0	Aluminum	0.125	No data	Yes	Yes	Attenuation by wake	Low frequency wake signal, ~50-percent cutoff of transmission, small signal from parasite horn
1425	26,700	20.0	Aluminum	0.125	0.71	Yes	Yes	Attenuation by wake	Low frequency wake signal; ~50-percent cutoff of transmission; small signal from parasite horn

Note: Horizontal position of model was well within the depth of focus of the microwave antenna in all shots.

*Model velocity measured between shadowgraph stations 2 and 3

†Blast tank pressure and range pressure equal except where noted

**Vertical distance from center of model to microwave beam axis (location of model was determined from shadowgraph station No. 2)

▲Velocity measured between s.g. stations 2-6

‡Figure in parenthesis is the blast tank pressure.

UNCLASSIFIED

Security Classification

DOCUMENT CONTROL DATA - R&D

(Security classification of title, body of abstract and indexing annotation must be entered when the overall report is classified)

1 ORIGINATING ACTIVITY *(Corporate author)*
Arnold Engineering Development Center
ARO, Inc., Operating Contractor
Arnold Air Force Station, Tennessee

2a REPORT SECURITY CLASSIFICATION
UNCLASSIFIED

2b GROUP
N/A

3 REPORT TITLE

RADAR STUDY OF SPHERE WAKES

4 DESCRIPTIVE NOTES *(Type of report and inclusive dates)*
N/A

5 AUTHOR(S) *(Last name, first name, initial)*

Hendrix, R. E. and Bailey, A. B., ARO, Inc.

6 REPORT DATE	7a TOTAL NO OF PAGES	7b NO OF REFS
November 1966	45	13

8a CONTRACT OR GRANT NO
AF40(600)-1200

b PROJECT NO

c Program Element 65402234

d

9a ORIGINATOR'S REPORT NUMBER(S)
AEDC-TR-66-182

9b OTHER REPORT NO(S) *(Any other numbers that may be assigned this report)*
N/A

10 AVAILABILITY/LIMITATION NOTICES
This document is subject to special export controls and each transmittal to foreign governments or foreign nationals may be made only with prior approval of AEDC (AETS), Arnold AF Station, Tennessee.

11 SUPPLEMENTARY NOTES
Available in DDC

12 SPONSORING MILITARY ACTIVITY
Arnold Engineering Development Center, Air Force Systems Command, Arnold Air Force Station, Tennessee

13 ABSTRACT

A series of firings was executed in the 100-ft Range K of the VKF for the purpose of determining the causes of radar reflections from the wakes of hypervelocity spheres. A 35-kmc, focused, oblique radar was employed as the primary instrumentation. In addition, receiving and parasite antennas were used to measure transmission and specular reflection. The results of these experiments indicate that, when using the 35-kmc microwave equipment described here, a detectable radar reflection in most cases was obtained from the wake of a hypervelocity sphere (10,000 to 27,000 ft/sec in these experiments) only if the sphere ablated. Measurements of turbulent wake velocity were shown to agree with the predicted values. The region of transition from laminar to turbulent flow was also defined.

DD FORM 1 JAN 64 1473

UNCLASSIFIED

Security Classification

14. KEY WORDS	LINK A		LINK B		LINK C	
	ROLE	WT	ROLE	WT	ROLE	WT
radar reflections						
sphere wakes						
antennas						
ablation						
hypervelocity						

INSTRUCTIONS

1. ORIGINATING ACTIVITY: Enter the name and address of the contractor, subcontractor, grantee, Department of Defense activity or other organization *(corporate author)* issuing the report.

2*a*. REPORT SECURITY CLASSIFICATION: Enter the overall security classification of the report. Indicate whether "Restricted Data" is included. Marking is to be in accordance with appropriate security regulations.

2*b*. GROUP: Automatic downgrading is specified in DoD Directive 5200.10 and Armed Forces Industrial Manual. Enter the group number. Also, when applicable, show that optional markings have been used for Group 3 and Group 4 as authorized.

3. REPORT TITLE: Enter the complete report title in all capital letters. Titles in all cases should be unclassified. If a meaningful title cannot be selected without classification, show title classification in all capitals in parenthesis immediately following the title.

4. DESCRIPTIVE NOTES: If appropriate, enter the type of report, e.g., interim, progress, summary, annual, or final. Give the inclusive dates when a specific reporting period is covered.

5. AUTHOR(S): Enter the name(s) of author(s) as shown on or in the report. Enter last name, first name, middle initial. If military, show rank and branch of service. The name of the principal author is an absolute minimum requirement.

6. REPORT DATE: Enter the date of the report as day, month, year; or month, year. If more than one date appears on the report, use date of publication.

7*a*. TOTAL NUMBER OF PAGES: The total page count should follow normal pagination procedures, i.e., enter the number of pages containing information.

7*b*. NUMBER OF REFERENCES: Enter the total number of references cited in the report.

8*a*. CONTRACT OR GRANT NUMBER: If appropriate, enter the applicable number of the contract or grant under which the report was written.

8*b*, 8*c*, & 8*d*. PROJECT NUMBER: Enter the appropriate military department identification, such as project number, subproject number, system numbers, task number, etc.

9*a*. ORIGINATOR'S REPORT NUMBER(S): Enter the official report number by which the document will be identified and controlled by the originating activity. This number must be unique to this report.

9*b*. OTHER REPORT NUMBER(S): If the report has been assigned any other report numbers *(either by the originator or by the sponsor)*, also enter this number(s).

10. AVAILABILITY/LIMITATION NOTICES: Enter any limitations on further dissemination of the report, other than those imposed by security classification, using standard statements such as:

(1) "Qualified requesters may obtain copies of this report from DDC."

(2) "Foreign announcement and dissemination of this report by DDC is not authorized."

(3) "U. S. Government agencies may obtain copies of this report directly from DDC. Other qualified DDC users shall request through

_____."

(4) "U. S. military agencies may obtain copies of this report directly from DDC. Other qualified users shall request through

_____."

(5) "All distribution of this report is controlled. Qualified DDC users shall request through

_____."

If the report has been furnished to the Office of Technical Services, Department of Commerce, for sale to the public, indicate this fact and enter the price, if known.

11. SUPPLEMENTARY NOTES: Use for additional explanatory notes.

12. SPONSORING MILITARY ACTIVITY: Enter the name of the departmental project office or laboratory sponsoring *(paying for)* the research and development. Include address.

13. ABSTRACT: Enter an abstract giving a brief and factual summary of the document indicative of the report, even though it may also appear elsewhere in the body of the technical report. If additional space is required, a continuation sheet shall be attached.

It is highly desirable that the abstract of classified reports be unclassified. Each paragraph of the abstract shall end with an indication of the military security classification of the information in the paragraph, represented as *(TS), (S), (C), or (U)*

There is no limitation on the length of the abstract. However, the suggested length is from 150 to 225 words.

14. KEY WORDS: Key words are technically meaningful terms or short phrases that characterize a report and may be used as index entries for cataloging the report. Key words must be selected so that no security classification is required. Identifiers, such as equipment model designation, trade name, military project code name, geographic location, may be used as key words but will be followed by an indication of technical context. The assignment of links, rules, and weights is optional.